JCB Journal of Cell Biology

ARTICLE

Effector-mediated ERM activation locally inhibits RhoA activity to shape the apical cell domain

Riasat Zaman*, Andrew Lombardo*, Cécile Sauvanet, Raghuvir Viswanatha, Valerie Awad, Locke Ezra-Ros Bonomo, David McDermitt, and Anthony Bretscher

Activated ezrin-radixin-moesin (ERM) proteins link the plasma membrane to the actin cytoskeleton to generate apical structures, including microvilli. Among many kinases implicated in ERM activation are the homologues LOK and SLK. CRISPR/Cas9 was used to knock out all ERM proteins or LOK/SLK in human cells. LOK/SLK knockout eliminates all ERM-activating phosphorylation. The apical domains of cells lacking LOK/SLK or ERMs are strikingly similar and selectively altered, with loss of microvilli and with junctional actin replaced by ectopic myosin-II–containing apical contractile structures. Constitutively active ezrin can reverse the phenotypes of either ERM or LOK/SLK knockouts, indicating that a central function of LOK/SLK is to activate ERMs. Both knockout lines have elevated active RhoA with concomitant enhanced myosin light chain phosphorylation, revealing that active ERMs are negative regulators of RhoA. As RhoA-GTP activates LOK/SLK to activate ERM proteins, the ability of active ERMs to negatively regulate RhoA-GTP represents a novel local feedback loop necessary for the proper apical morphology of epithelial cells.

Introduction

Essentially all eukaryotic cells are, or have the potential to become, polarized. This requires local regulation to define the morphology and composition of each domain. A well-studied case is the polarized epithelial cell with an apical domain displaying abundant microvilli and having a protein and lipid composition distinct from the basolateral membrane. While much is known about extrinsic cues that instruct cell polarization (Rodriguez-Boulan and Macara, 2014), less is known about how the morphology of the individual domains is regulated. To address this, we have studied how the apical domain is regulated to assemble bundles of actin filaments that support the plasma membrane of microvilli.

The structural integrity of apical microvilli requires active ezrin-radixin-moesin (ERM) proteins (Fehon et al., 2010). These proteins exist in a cytoplasmic closed state and an active open conformation where the N-terminal FERM (4.1 protein ERM) domain binds the plasma membrane and the C-terminal F-actin binding domain binds the underlying actin filaments (Gary and Bretscher, 1995). Activation requires phosphorylation of a conserved threonine, T567, in ezrin (Hayashi et al., 1999; Matsui et al., 1998). Among the many kinases suggested to be responsible for ERM phosphorylation are Rho-associated protein kinase (ROCK; Matsui et al., 1998; Tran Quang et al., 2000; Haas et al., 2007), PKCα (Ng et al., 2001), PKCϑ (Pietromonaco et al., 1998), MST4 (Gloerich et al., 2012; ten Klooster et al., 2009), NcK-interacting kinase (Baumgartner et al., 2006), and lymphocyte-oriented kinase (LOK; Belkina et al., 2009; Viswanatha et al., 2012). More recent evidence has suggested that the related LOK and STE20-like serine/threonine-protein kinase (SLK) are major vertebrate kinase activators for ERM phosphorylation (Viswanatha et al., 2012). LOK and SLK are the homologues of the fly *Drosophila melanogaster* kinase Slik (Sterile20-like kinase) that is responsible for phosphorylating the single fly ERM, moesin (Hipfner et al., 2004). Both LOK-GFP and SLK-GFP have been shown to target to the apical membrane where ERMs are activated (Viswanatha et al., 2012). LOK and SLK belong to the germinal center–like kinase V subfamily (Kuramochi et al., 1997). They consist of a conserved N-terminal kinase domain, a less-conserved intermediate region, and a moderately conserved C-terminal domain (CTD). The LOK CTD inhibits the kinase activity of LOK in cells, most likely through a *cis* interaction, as well as targeting LOK to the apical membrane (Pelaseyed et al., 2017; Viswanatha et al., 2012). Constitutively active ezrin is unable to maintain apical

Department of Molecular Biology and Genetics, Weill Institute for Cell and Molecular Biology, Cornell University, Ithaca, NY.

*R. Zaman and A. Lombardo contributed equally to this paper; Correspondence to Anthony Bretscher: apb5@cornell.edu; C. Sauvanet's present address is Unit of Structural Studies of Macromolecular Machines in Cellula, Department of Structural Biology and Chemistry, Institut Pasteur, Centre national de la recherche scientifique, Unité mixte de recherche 3528, Paris, France; R. Viswanatha's present address is Blavatnik Institute of Genetics, Harvard Medical School, Boston, MA.

restriction because ezrin has to undergo phosphorylation/dephosphorylation cycles in which it is locally phosphorylated and subject to dephosphorylation by delocalized myosin phosphatase target subunit 1/protein phosphatase 1 (Mypt1/PP1; Jin et al., 2006).

The Rho family of small GTP-binding proteins are major regulators of microfilaments (Hall and Nobes, 2000). In early work, Speck et al. (2003) found that defects in fly moesin could be counteracted by antagonizing Rho activity, suggesting that ERM proteins might be able to regulate contractility in some manner. Additionally, they found that expression of a dominant negative ezrin resulted in elevated active RhoA levels in cultured porcine cells. Active RhoA binds a diverse range of effectors that influence the reorganization of actin into contractile fibers and focal adhesions (Hall, 1998). Among these, the effector ROCK modulates microfilament organization and function in at least two distinct ways. First, it activates myosin-II by directly phosphorylating the myosin regulatory light chain (Amano et al., 1996) and inactivating Mypt1/PP1 (Kimura et al., 1996). Second, ROCK stabilizes F-actin by phosphorylating LIM kinase to abrogate its inhibitory activity toward cofilin, an F-actin destabilizing factor (Arber et al., 1998; Maekawa et al., 1999; Yang et al., 1998). The net effect results in an increase of cortical tension that can drive cellular contraction. ERM proteins have long been suggested to be downstream targets of ROCK, first as direct targets and then as indirect targets through Rho activation of phosphatidylinositol 4-phosphate 5-kinase (Matsui et al., 1998, 1999).

Recently, a BioID screen for regulators and effectors of RhoA in cultured cells identified SLK and LOK as effectors of RhoA (Bagci et al., 2020). RhoA-GTP binds the CTD of SLK, the corresponding domain that negatively regulates the kinase activity and targets LOK to the apical domain (Bagci et al., 2020). Moreover, active RhoA can activate SLK in its ability to phosphorylate ezrin. Thus, a direct pathway exists from RhoA-GTP to its effector LOK/SLK to ERM protein activation.

Further uncovering the functions and exploring signaling pathways related to ERM proteins and LOK and SLK in cultured cells has been hampered by redundancy and the possibility that they perform essential functions. Here we describe the generation of cultured cells lacking all ERM proteins and cells lacking both LOK and SLK. Surprisingly, cells lacking LOK and SLK have a strikingly similar phenotype to cells lacking ERM proteins. Our results establish that LOK and SLK are the major, and possibly only, kinases that phosphorylate the conserved threonine of ERM proteins in epithelial cells. Further, rescue experiments indicate that ERM proteins are the major substrates of LOK and SLK that regulate cell morphology. Moreover, loss of either LOK/SLK or ERM proteins elevates RhoA signaling to redistribute actin from microvilli and junctions to generate ectopic apical contractile fibers. We propose that LOK/SLK and ERM proteins function as a module that defines apical morphology of epithelial cells in a process that involves a negative feedback loop to locally downregulate Rho activity.

Results

Jeg-3 cells lacking ERM proteins or LOK/SLK are viable and lack microvilli

We have described human cells modified by CRISPR/Cas9 to lack expression of LOK (Pelaseyed et al., 2017), but so far no cultured cells have been described that genetically lack specific ERM proteins. We set out to determine if cells lacking all ERM proteins, or lacking both LOK and SLK, are viable and, if so, what phenotypes were conferred. We used Jeg-3 epithelial cells derived from a human choriocarcinoma as they exhibit abundant apical microvilli (Pakkanen et al., 1987). Of the ERM proteins, Jeg-3 cells express ezrin and radixin, but not moesin (Fig. 1 A). We first used CRISPR/Cas9 to isolate single-knockout cells lacking either ezrin, radixin, LOK, or SLK (Fig. 1 A). These single-knockout lines showed no significant compensation in the levels of the remaining ERMs or LOK/SLK kinase (Fig. S1 A). We then generated pairs of double-knockout cells lacking all detectable ezrin and radixin or LOK and SLK (Fig. 1 A). Importantly, moesin was not expressed in the Jeg-3 ezrin$^{-/-}$ radixin$^{-/-}$ cells, which can be identified as moesin being expressed in HeLa cells (Fig. 1 A, lane 1). Thus, Jeg-3 cells lacking all ERM proteins or both LOK and SLK are viable but grow slower than their wild-type counterparts (Fig. S1 B).

As ERM proteins and LOK and SLK have been implicated in the formation of microvilli, we examined whether single- and double-knockout cells retained microvilli. To assess the presence of microvilli, we could not use the traditional ERM proteins as markers, so we used labeled wheat germ agglutinin (WGA) that binds to plasma membrane glycoproteins and allows the identification of cell surface structures. In wild-type cells, WGA colocalizes with ezrin in surface microvilli (Fig. 1 B). Consistent with earlier reports, individual reduction of ezrin or genetic loss of LOK resulted in a reduced number of cells with apical microvilli, whereas loss of radixin or SLK had little phenotype (Fig. 1 C and Fig. S1 C; Bonilha et al., 1999; Pelaseyed et al., 2017). Strikingly, ezrin$^{-/-}$ radixin$^{-/-}$ and LOK$^{-/-}$ SLK$^{-/-}$ cells totally lack microvilli, with WGA staining mostly associated with membrane ruffles that form above membrane contact sites (Fig. 1 B, arrows). Ezrin is cytosolic in LOK$^{-/-}$ SLK$^{-/-}$ cells, consistent with phosphorylation by LOK/SLK being required to activate it. Stable expression of ezrin in ezrin$^{-/-}$ radixin$^{-/-}$ cells and LOK in LOK$^{-/-}$/SLK$^{-/-}$ cells (Fig. S1 D) restored the presence of microvilli to the cell surface (Fig. 1 B). We also examined the localization of the interactor of active ezrin, ERM-binding phosphoprotein of 50 kD (EBP50)/NHERF1. Whereas EBP50 was present in microvilli in wild-type cells, in both double-knockout cell lines, EBP50 was cytosolic (Fig. 1 D). An ERM protein and LOK or SLK are therefore necessary for the presence of apical microvilli.

LOK/SLK are the major kinases for ERM phosphorylation

ERM proteins undergo activation by C-terminal phosphorylation to exhibit their membrane–cytoskeleton linking function (Nakamura et al., 1995; Pearson et al., 2000). The identity of the relevant kinase has been controversial, so we assessed the contribution of LOK and SLK to ERM phosphorylation in LOK$^{-/-}$ SLK$^{-/-}$ cells. As reported for expressed LOK-GFP (Viswanatha et al., 2012), endogenous LOK is apically localized, with enrichment in microvilli (Fig. 2 A). Using an antibody that detects the relevant phospho-epitope on all ERM proteins (phosphorylation of T567 in ezrin, T564 in radixin, and T558 in moesin), we found that LOK$^{-/-}$ SLK$^{-/-}$ cells appeared devoid of ERM phosphorylation (Fig. 2 B). However, because the phosphorylated ERM (pERM) antibody produces a small background

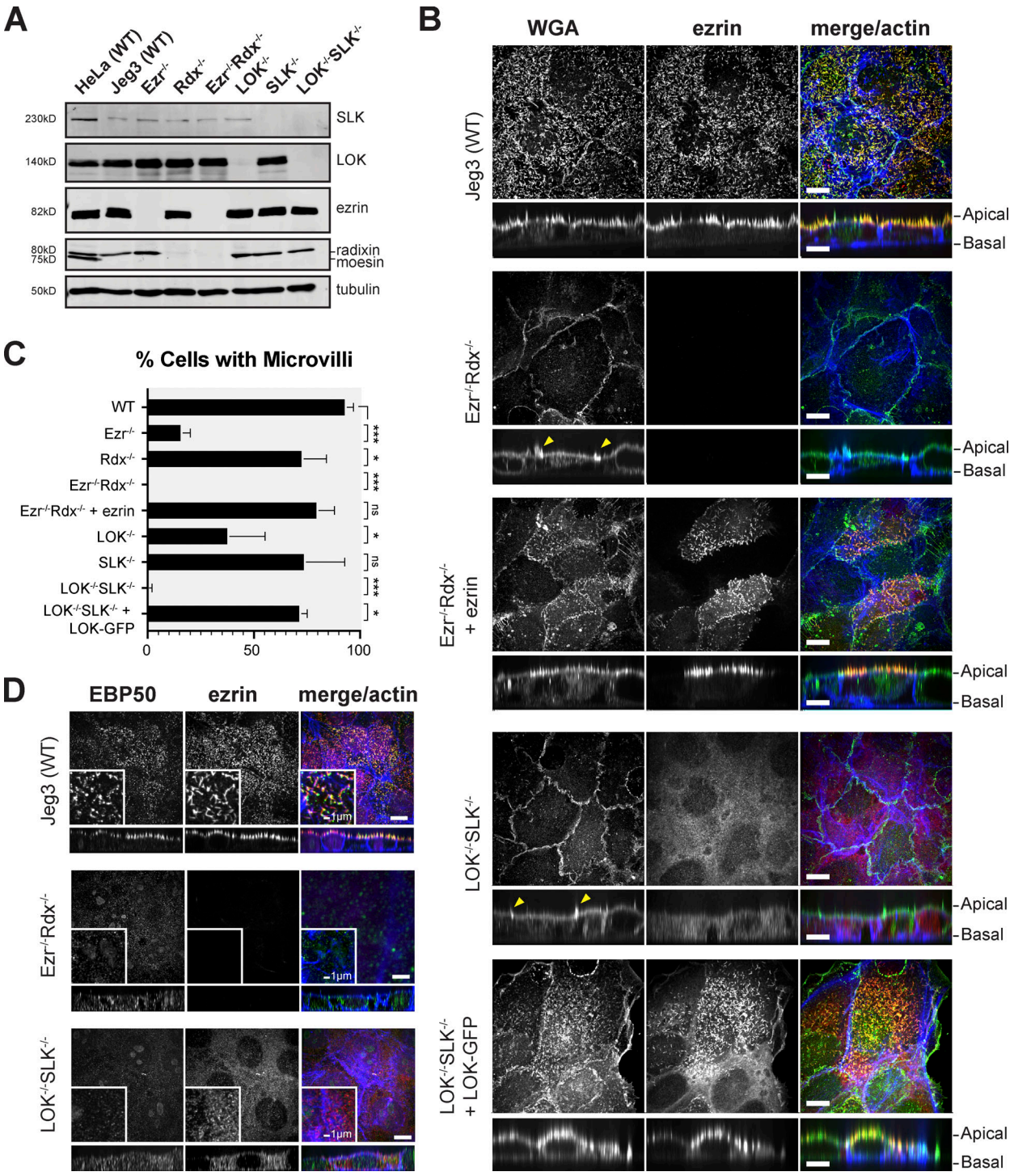

Figure 1. **Jeg-3 cells lacking ERM proteins or LOK/SLK are viable and lack microvilli. (A)** Protein expression using the indicated antibodies in Western blots of ERM proteins and LOK and SLK in Jeg-3 CRISPR cell lysates. HeLa cell lysate was used as a control for expression of moesin, which is not present in Jeg-3. Tubulin expression was used as a loading control. **(B)** Jeg-3 cell lines lacking ERM expression or LOK and SLK expression were stained with WGA, ezrin, and actin. Yellow arrowheads indicate strong membrane ruffles. **(C)** Percentage of cells expressing microvilli. Bars represents mean ± SEM; $n = 3$. P values were calculated with Welch's t test (*, $P \le 0.05$; ***, $P \le 0.001$). **(D)** Staining of cells with EBP50, ezrin, and actin in the indicated cells. Scale bars, 10 µm unless otherwise noted. Vertical sections were expanded threefold for clarity.

staining to unphosphorylated ezrin (Pelaseyed et al., 2017), we repeated the experiment using Phos-tag gels in which pERMs migrate slower than their unphosphorylated counterparts. Again, we were unable to detect any pERM proteins in the absence of LOK and SLK (Fig. 2 C), so LOK and SLK are the only significant ERM kinases in Jeg-3 cells.

To explore if this is true in other cells, we generated LOK$^{-/-}$ SLK$^{-/-}$ knockouts in HeLa cells. While these cells survived clonal

isolation and lysate collection, they grew very slowly and could not be maintained. Nevertheless, analysis of cell lysates revealed that in HeLa cells LOK and SLK are the major ERM kinases (Fig. 2 B). As shown later in the results (see Fig. 8), knockout of LOK/SLK in intestinal DLD-1 cells also showed that LOK/SLK are the major ERM kinases. Further, we tried to knock out LOK and SLK in epithelial Caco-2 cells, which proved inviable past clonal selection, indicating the importance of these kinases. Likewise, we tried to isolate HeLa and Caco-2 cells lacking ezrin. Although we nursed the growth of enough cells to demonstrate loss of ezrin, they could not be passaged. These results suggest that ERM proteins are more important for viability in HeLa and Caco-2 cells than in Jeg-3 cells. It was fortuitous that we started with Jeg-3 cells as it allowed us to use the double knockouts to explore the phenotypes conferred by loss of these proteins.

In transfection-based experiments, expression of LOK-GFP-Flag was able to restore both apical microvilli and ERM phosphorylation to LOK$^{-/-}$ SLK$^{-/-}$ cells (Fig. 1, B and C; and Fig. 2 D). LOK contains an N-terminal kinase domain and a CTD responsible for both regulating and localizing the kinase (Pelaseyed et al., 2017). As expected, expression of a K65R kinase-inactive variant of LOK was unable to restore phosphorylation or microvilli (Fig. 2, D and E).

Absence of activated ERM proteins induces the formation of apical actin/myosin-II bundles and alters cell–cell junctions of epithelial cells

To explore novel phenotypes that might be associated with the loss of ERM proteins or their activating kinases, we examined other aspects of the apical domain, notably cell junctions. A characteristic feature of wild-type epithelial cells is their ability to form strong apical cell-to-cell contact sites, with relatively straight tight junctions marked by ZO-1 and actin and E-cadherin associated with adherens junctions (Fig. 3, A and B; and Fig. S2 A). In contrast, ezrin$^{-/-}$ radixin$^{-/-}$ and LOK$^{-/-}$ SLK$^{-/-}$ cells had a remarkably similar phenotype. The cells have uneven contact sites, occasionally with breaks in their ZO-1 staining, and have greatly reduced junctional actin staining, whereas basal actin is largely unchanged (Fig. 3, A and B). By determining the ratio between the contour length and shortest distance in ZO-1 staining from a three-cell junction to the next, we quantified the straightness of the tight junctions (Fig. 3 C). This measurement of tortuosity was slightly above 1.0 for wild-type cells, reflecting their almost linear nature. For either ezrin$^{-/-}$ or LOK $^{-/-}$, this rose to 1.15, and for ezrin$^{-/-}$ radixin$^{-/-}$ and LOK$^{-/-}$/SLK$^{-/-}$ cells to ∼1.2, indicating greater distortion/waviness of the interface. As with loss of microvilli, loss of just ezrin or LOK is more severe than loss of just radixin or SLK, and both double mutants exhibit the most severe phenotype. This tortuosity of the junctions was rescued by expressing ezrin in the ezrin$^{-/-}$ radixin$^{-/-}$ cells and LOK-GFP in the LOK$^{-/-}$ SLK$^{-/-}$ cells (Fig. 3, A and C). By following expressed ZO-1–GFP in dividing cells, the uneven ZO-1 localization in both ezrin$^{-/-}$ radixin$^{-/-}$ and LOK$^{-/-}$/SLK$^{-/-}$ cells was found to develop shortly after cell division (Fig. S2 B and Video 1).

We also noticed a striking effect on the actin distribution, with more F-actin spanning the apical domain in the double-knockout cells compared with their wild-type counterpart. Therefore, we examined the F-actin distribution in the basal and apical regions of the cells separately. ZO-1 localization is found near the apical region of both wild-type and knockout cells, so we split confocal planes into those containing ZO-1 staining and above (the apical domain) and those below ZO-1 staining (the basolateral domain). Whereas the wild-type cells display actin in microvilli and along the cell junctions, both ezrin$^{-/-}$ radixin$^{-/-}$ and LOK$^{-/-}$ SLK$^{-/-}$ cells had actin bundles extending across the apical domain that correlated with the uneven contour of the tight junctions (Fig. 3, A and C). We quantified this difference by measuring the ratio of the actin intensity at the apical versus the basal side of the cells (Fig. 3 D). Both knockout cells were found to have an increase in apical actin compared with wild-type cells (Fig. 3, A and D). The aberrant apical actin bundles are rescued by introduction of ezrin into ezrin$^{-/-}$ radixin$^{-/-}$ and of LOK-GFP into LOK$^{-/-}$ SLK$^{-/-}$ cells (Fig. 3, A, B, and D).

The apical actin bundles seen in knockout cells appear similar to stress fibers. The expression level of the stress fiber markers myosin-II and α-actinin and focal adhesion marker vinculin, and the basal localization of paxillin and vinculin, were unchanged in the knockout cells (Fig. S2, C–E). We next explored if the apical bundles could have contractile properties by imaging nonmuscle myosin-IIB (myo-IIB) using super-resolution structured illumination microscopy (SIM). While striated bundles of myo-IIB and actin were not completely absent in the apical region of wild-type cells, a stronger intensity and more frequent clusters of myo-IIB spanned the apical domain of ezrin$^{-/-}$ radixin$^{-/-}$ cells and LOK$^{-/-}$ SLK$^{-/-}$ cells (Fig. 4, A and B). A similar result was found when myo-IIA was imaged (Fig. S3 A). Imaging the midregion in ezrin$^{-/-}$ radixin$^{-/-}$ cells showed contractile bundles apparently pulling on junctional actin to generate the uneven junctions (Fig. 4 C). Together, our results show that lack of activated ERMs, due to loss of either the proteins or their activating kinases, selectively redistributes actin in the apical domain into contractile bundles. To see if inhibition of contractility restored normal junctions, we treated cells with the myosin-II inhibitor blebbistatin. This treatment yielded similar phenotypes for wild-type and knockout cells, but the interpretation is complicated by the effect that blebbistatin has on the wild-type controls (Figs. S3, B and C).

To assess how the actin redistribution might affect the mechanics of the apical surface, we used atomic force microscopy (AFM) to measure cells' stiffness. Cells were grown to a confluent monolayer and then indented to a maximum force of 1 nN (Fig. 4 D, inset). The resulting force versus distance curves were then used to identify the initial AFM probe tip contact point, allowing us to fit to a Hertz equation to calculate the Young's modulus (E) stiffness parameter (Huth et al., 2019). Indentations from each condition were then averaged to produce a mean curve for wild-type, ezrin$^{-/-}$ radixin$^{-/-}$, and LOK$^{-/-}$ SLK$^{-/-}$ cells (Fig. 4 D). Of the 1,091 total force indentations performed, both LOK$^{-/-}$ SLK$^{-/-}$ (E = 260 ± 45 kPa mean ± SD) and ezrin$^{-/-}$ radixin$^{-/-}$ (E = 166 ± 52 kPa) cells were significantly stiffer than wild-type cells (E = 117 ± 65 kPa; Fig. 4 E). The finding that LOK$^{-/-}$ SLK$^{-/-}$ cells are more rigid than ezrin$^{-/-}$ radixin$^{-/-}$ cells is consistent with the enhanced levels of contractile bundles

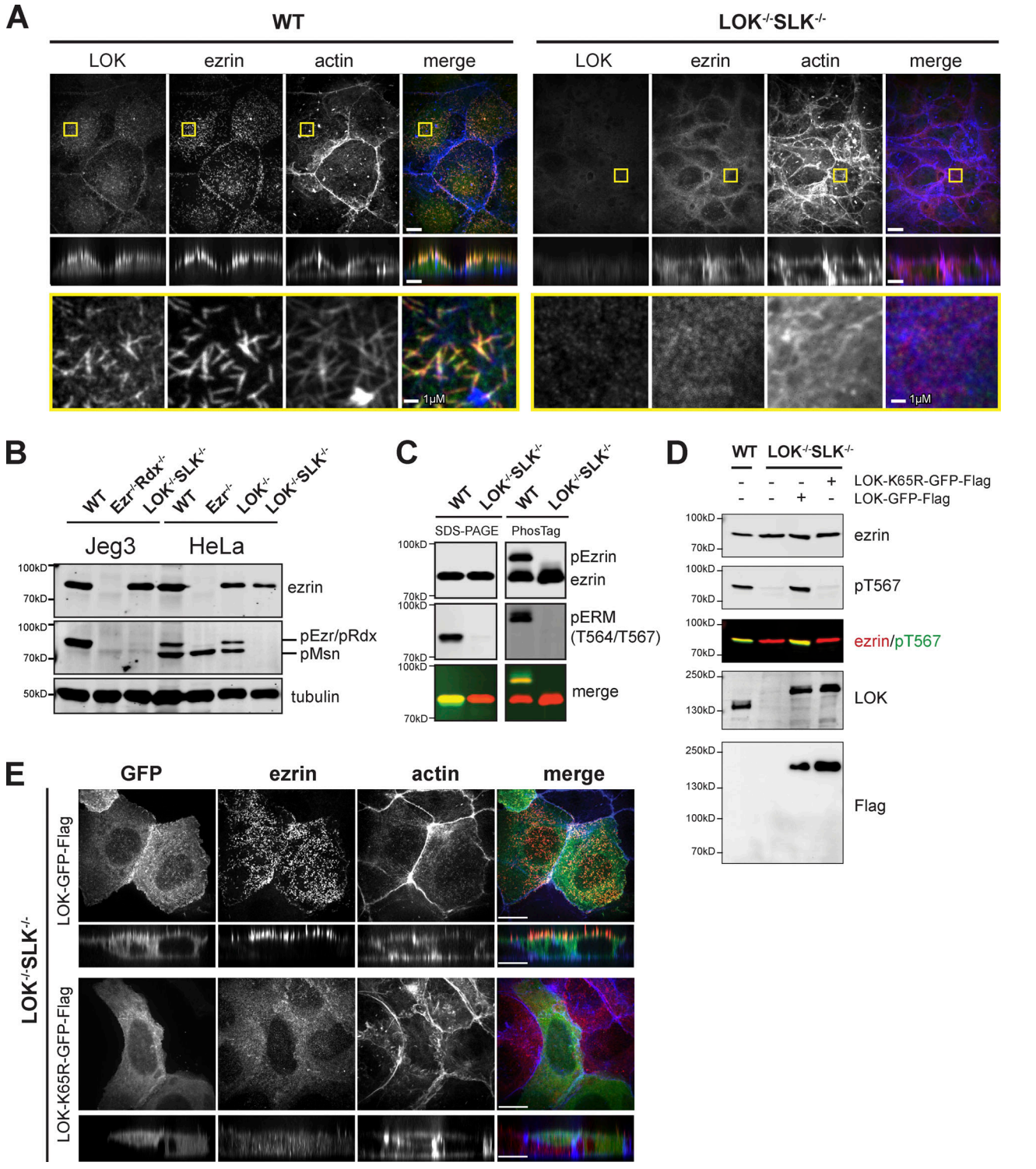

Figure 2. **LOK/SLK are the major ERM kinases. (A)** Localization of endogenous LOK, ezrin, and actin in Jeg-3 wild-type and LOK$^{-/-}$ SLK$^{-/-}$cells. Images are max projections except for yellow boxes, which represent magnification of apical Z-slices. **(B)** Ezrin and pERM levels in Jeg-3– or HeLa-knockout cells. Tubulin is used as a loading control. **(C)** Extracts of wild-type or LOK$^{-/-}$ SLK$^{-/-}$ cells were resolved by either 6% SDS-PAGE gel or 6% Mn-Phos-tag SDS-PAGE gel and blotted for ezrin and pERM. Approximately half of endogenous ezrin is phosphorylated in wild-type cells, as seen by the band shift. No phospho-shift is detected in LOK$^{-/-}$ SLK$^{-/-}$ cells. **(D)** Extracts of cells transfected with wild-type LOK or LOK mutants were collected and blotted for endogenous, untagged ezrin or pERM. Lysates were also blotted for Flag or LOK to check expression of the constructs relative to wild-type LOK. **(E)** LOK$^{-/-}$ SLK$^{-/-}$ cells were transfected with either LOK-GFP-Flag or K65R-LOK-GFP-Flag and then costained with ezrin and actin. K65R-LOK is unable to rescue apical ezrin localization. Vertical sections were expanded threefold for clarity. Scale bars, 10 µm unless otherwise noted in magnified sections.

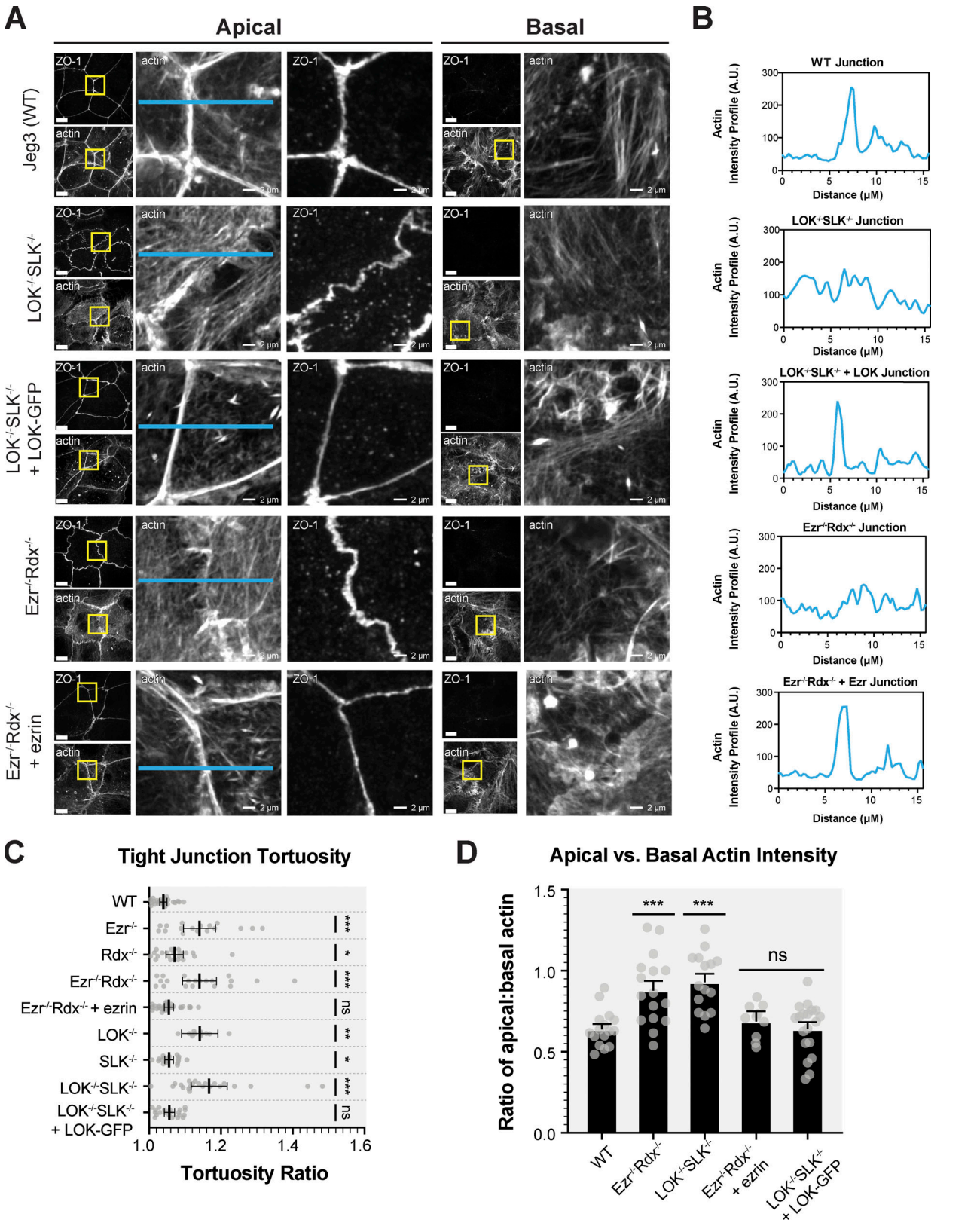

Figure 3. **Absence of activated ERM proteins alters cell–cell junctions. (A)** Comparison of ZO-1 and actin between apical and basolateral confocal slices. Apical Z-slices were determined by the presence of ZO-1. Scale bars, 10 µm unless otherwise noted in magnified images (2 µm). **(B)** Intensity of actin across junctions highlighted in blue in A. **(C)** Quantification of tight junction tortuosity using ZO-1 staining. Each point represents the tortuosity from one tight junction intersection to the next intersection. Center lines represent mean ± SEM; $n \geq 10$ cells per condition. **(D)** The ratios of relative mean actin intensity values per cell between apical and basolateral cross-sections. Bars represent mean ± SEM; $n \geq 10$ cells per condition. P values were calculated with Welch's *t* test (*, $P \leq 0.05$; **, $P \leq 0.01$; ***, $P \leq 0.001$). A.U., arbitrary units.

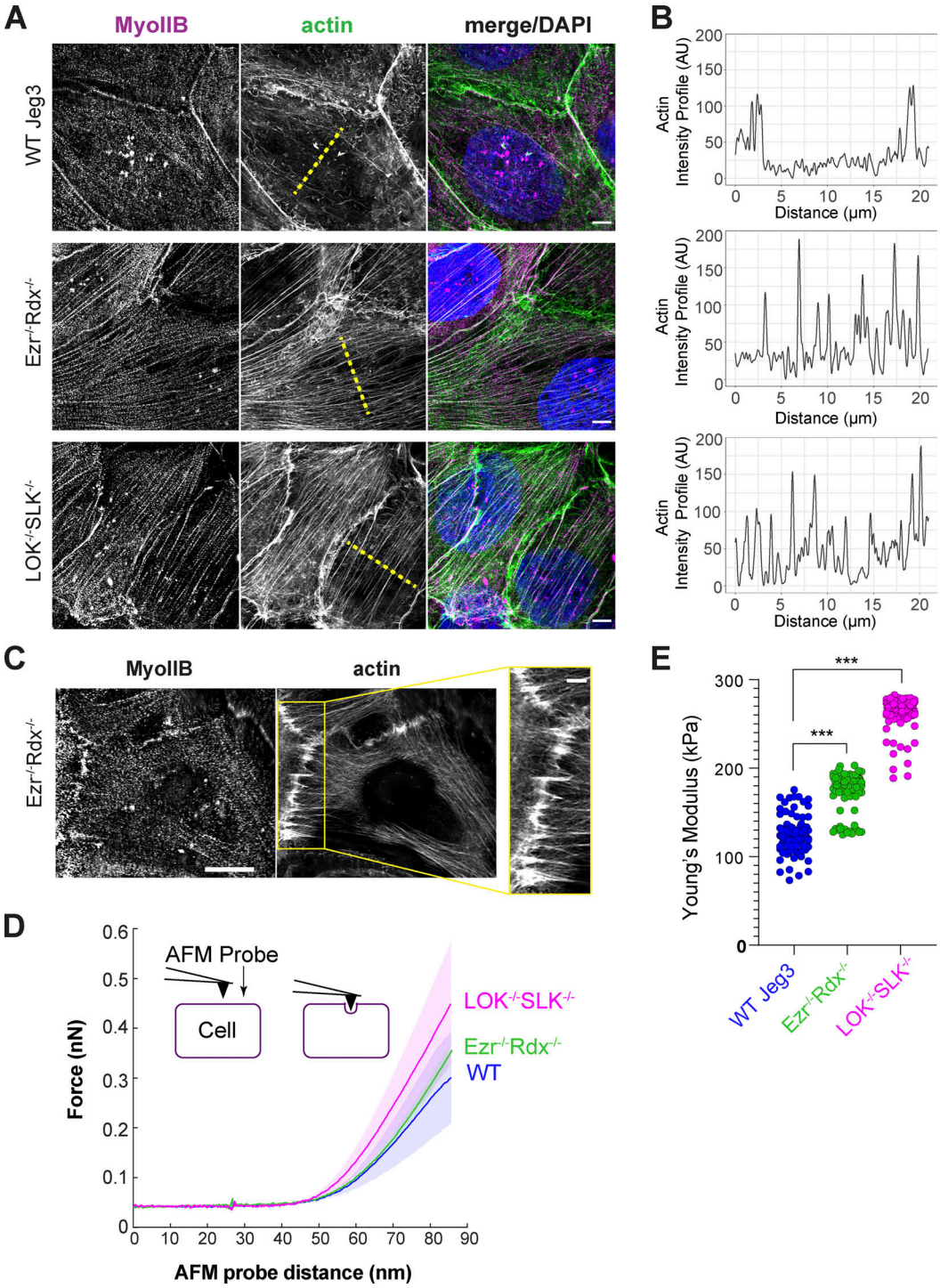

Figure 4. **A dense actomyosin network forms at the apical surface of ERM- and LOK/SLK-knockout cells. (A)** Representative SIM reconstructions of the apical surface of Jeg-3 cells labeled with anti–myo-IIB, phalloidin, and DAPI. Scale bars, 5 µm. **(B)** Line scans of the actin intensity across the center of the apical surface of each cell type shown as dotted yellow lines in A. **(C)** Example stacked SIM Z-slices from the middle of $Ezr^{-/-}Rdx^{-/-}$ cells labeled with anti–myo-IIB and Alexa Fluor 647 phalloidin. Zoom-in highlighting the attachment of the apical contractile fibers to the cell–cell junctions. Scale bars, 5 µm; inset, 2 µm. **(D)** Averaged force indentation curves for wild-type Jeg-3 (blue), $Ezr^{-/-}$ $Rdx^{-/-}$ (green), and $LOK^{-/-}$ $SLK^{-/-}$ (magenta); semitransparent area around each line represents the SEM of the data. A steeper curve indicates a stiffer cell. **(E)** Young's modulus stiffness parameters. Black line indicates each condition's mean value (wild type, n = 356; $Ezr^{-/-}$ $Rdx^{-/-}$, n = 304; $LOK^{-/-}$ $SLK^{-/-}$, n = 431). Both knockout conditions were significantly stiffer than wild-type cells (***, $P \leq 0.0001$, Kolmogorov-Smirnov test). AU, arbitrary units.

seen in the apical domain of LOK$^{-/-}$ SLK$^{-/-}$ cells. Together, these results indicate that activated ERM proteins suppress the formation of apical actin bundles to affect the mechanical properties of the apical domain.

Enhanced actin assembly in the apical domain is responsible for the junctional defects of knockout cells

In wild-type cells, apical actin in the microvilli treadmills continuously resulted in turnover in ∼2–10 min (Loomis et al., 2003; Meenderink et al., 2019). We investigated the possibility that the abnormal actin bundles seen in knockout cells might arise in part from reduced actin turnover in the apical domain. To test this, we treated wild-type cells with the actin-stabilizing drug jasplakinolide to reduce actin turnover. Remarkably, treatment of wild-type cells with 500 nM jasplakinolide for 30 min both induced the formation of actin bundles in the apical domain and increased the tortuosity of the tight junctions (Fig. 5, A and B) in a manner closely resembling the phenotype of ezrin$^{-/-}$ radixin$^{-/-}$ or LOK$^{-/-}$ SLK$^{-/-}$ cells (Fig. 3 A). The addition of jasplakinolide in all three cell lines further increased the abundance of apical F-actin networks across each cell, correlating with the increased tight junction tortuosity and breaks between neighboring cells (Fig. 5 A, magenta arrows; and Fig. 5 C).

If enhanced actin assembly in the double-knockout cells is responsible for the observed tortuosity of the junctions, increasing depolymerization in these cells might rescue this phenotype. Upon treatment of either of the double-knockout cells with the actin-depolymerizing drug latrunculin B or actin plus-end–capping drug cytochalasin D, tight junction tortuosity ratios in the knockout cells were restored to levels comparable to wild-type cells (Fig. 5, A and B; and Fig. S4 A). Interestingly, latrunculin B treatment of cells did not completely restore the balance of F-actin between the apical and basolateral domains to wild-type levels (Fig. 5 C). Analysis of the apical/basolateral actin distribution after these drug treatments was complicated by the finding that apical actin appears to be more resistant to disassembly by latrunculin B than its basolateral counterpart (Fig. S4 B). Nonetheless, in contrast to jasplakinolide-treated cells, latrunculin B treatment results in reorganization of actin toward junctions (Fig. 5 A, blue arrows) and relief of junctional defects (Fig. 5 B). Meanwhile, stabilization by jasplakinolide redistributes actin away from the junctions and across the cell, promoting junctional defects (Fig. 5, A and B). In summary, our data show that ezrin$^{-/-}$ radixin$^{-/-}$ and LOK$^{-/-}$ SLK$^{-/-}$ cells become more similar to wild-type cells when treated with latrunculin B, while wild-type cells become more like the knockout cells when treated with jasplakinolide. Therefore, in the absence of active ERMs, excessive actin assembly generates contractile bundles that provide forces perpendicular to junctions.

Activated ezrin rescues both ezrin$^{-/-}$ radixin$^{-/-}$ and LOK$^{-/-}$ SLK$^{-/-}$ cells

The phenotypic similarity of the ezrin$^{-/-}$ radixin$^{-/-}$ and LOK$^{-/-}$ SLK$^{-/-}$ cells suggested that essentially all the phenotypes of LOK$^{-/-}$ SLK$^{-/-}$ cells are due to the lack of ERM phosphorylation. If this is the case, introduction of mutationally activated ezrin in either of the double-knockout cells should rescue them in a similar manner. We therefore introduced the constitutively active phosphomimetic ezrin-T567D mutant into both ezrin$^{-/-}$ radixin$^{-/-}$ and LOK$^{-/-}$ SLK$^{-/-}$ cells. Remarkably, phosphomimetic ezrin suppressed both equally with restoration of microvilli (Fig. 6, A and B). The rescue isn't perfect, as constitutively active ezrin is localized both apically and basolaterally because restriction to the apical domain requires ezrin phosphocycling (Viswanatha et al., 2012). Expression of constitutively active phosphomimetic ezrin-T567D is able to suppress tight junction defects and the excess apical actin bundles seen in knockout cells, implying that active ezrin can regulate actin at the cortex (Fig. 6, A–E). These results suggest that a primary role for LOK and SLK in Jeg-3 cells is to phosphorylate ERMs.

pERM proteins regulate myosin-II activity through RhoA activation

The appearance of apical contractile cables in cells lacking activated ERMs is suggestive of local enhanced RhoA activity. ROCK is a major effector of RhoA-GTP that can activate myosin-II by directly phosphorylating myosin light chain 2 (MLC2), and this is counteracted by the phosphatase PP1 using the Mypt1 subunit. Total nonmuscle myosin-II expression showed no differences between wild-type and LOK$^{-/-}$ SLK$^{-/-}$ or ezrin$^{-/-}$ radixin$^{-/-}$ cells (Fig. S2 C). The level of endogenous MLC2 phosphorylation was very low in wild-type cells and enhanced in both ezrin$^{-/-}$ radixin$^{-/-}$ and LOK$^{-/-}$ SLK$^{-/-}$ cells. This signal was sensitive to the ROCK inhibitor Y-27632 (Fig. 7, A and B). To enhance the level of phosphorylation, we treated cells briefly with calyculin A to inhibit the phosphatase PP1. Treatment of wild-type cells with calyculin A enhanced the level of MLC2 phosphorylation and greatly enhanced the level seen in both of the knockout lines, again being sensitive to the ROCK inhibitor (Fig. 7, A and B). Localization of apical phospho-MLC parallels these results: There is an enhanced level in both knockout cell lines, which is increased upon calyculin A treatment and abolished by Y-27632 treatment (Fig. 7 C). These results reveal that activated ERM proteins negatively regulate ROCK-mediated phosphorylation of MLC2.

We next assessed the level of endogenous RhoA-GTP by passing total cell lysates over rhotekin-GST beads and measuring the relative levels of RhoA retained. Both ezrin$^{-/-}$ radixin$^{-/-}$ and LOK$^{-/-}$ SLK$^{-/-}$ cells were found to have about a threefold higher level of endogenous active RhoA than wild-type cells (Fig. 7, D and E). This enhanced level of active RhoA seen in the knockout cells is partially insensitive to Y-27632, with the knockout cells containing higher levels of active RhoA than wild-type cells in the presence of Y-27632 (Fig. 7, D and E). Thus, the absence of activated ERM proteins elevates levels of active RhoA in a pathway independent of ROCK (Fig. 7 G). Additionally, in all the cells, the level of active RhoA was enhanced by the presence of Y-27632, indicating that ROCK itself can negatively regulate the level of active RhoA in an unknown pathway independent of active ERMs. In addition to regulating MLC2 phosphorylation, ROCK also regulates actin dynamics through the LIM kinase/cofilin pathway (Arber et al., 1998; Maekawa et al., 1999; Yang et al., 1998), which may explain in part the altered actin dynamics discussed earlier.

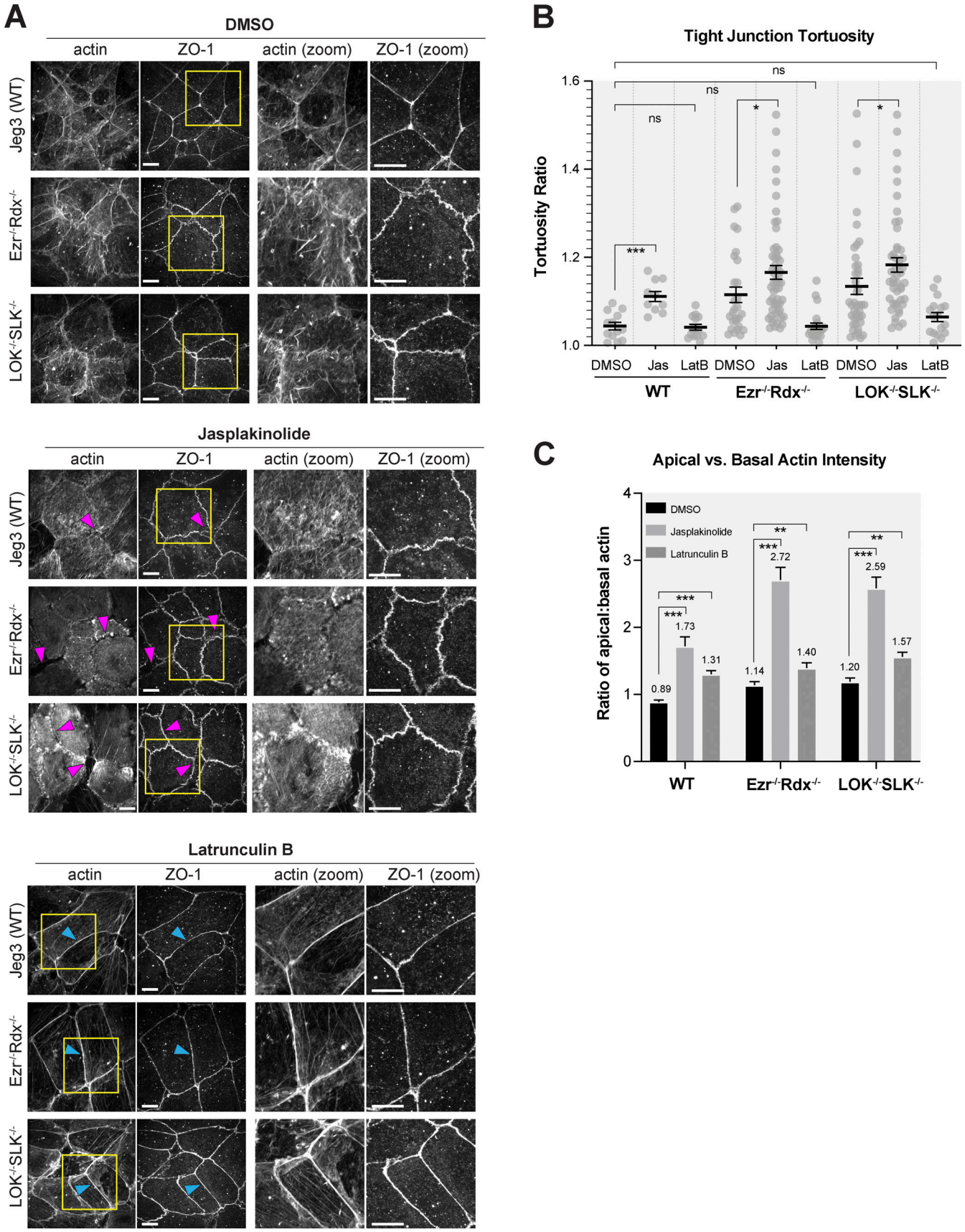

Figure 5. **Increased actin polymerization in ERM- or LOK/SLK-knockout cells leads to junctional defects. (A)** Jeg-3 cells treated with DMSO, 500 nM jasplakinolide, or 100 ng/ml latrunculin B for 30 min before immunostaining with ZO-1 and actin. Yellow boxes correspond with magnified images. Magenta

arrowheads point to actin gaps at junctions, while blue arrowheads represent actin present at cell junctions. Scale bars, 10 µm. **(B)** Quantification of tortuosity between tight junction markers as described in Fig. 3. Jasplakinolide (Jas) treatment increases tortuosity values, while latrunculin B (LatB) rescues tortuosity to wild-type levels. $n \geq 10$ cells per condition. Lines represent mean ± SEM. **(C)** Comparison of actin levels between apical and basolateral regions after treatment with drugs as visualized in A. $n \geq 21$ cells per condition. Bars show mean ± SEM. P values were calculated with Welch's t test (*, $P \leq 0.05$; **, $P \leq 0.01$; ***, $P \leq 0.001$).

A recent report showed that active RhoA binds directly to the CTD of SLK and that this promotes its ability to phosphorylate ERM proteins (Bagci et al., 2020). Earlier work showed that expression of the C-terminal region of LOK (LOK-CTD-GFP-Flag) acts as a potent dominant negative to strongly inhibit phosphorylation of ERM proteins (Viswanatha et al., 2012). To explore if this region of LOK binds to RhoA, we expressed LOK-CTD-GFP-Flag either alone or with constitutively active HA-RhoA-L30 and immunoprecipitated with Flag antibodies in wild-type Jeg-3 cells (Fig. 7 F). RhoA was recovered in the Flag immunoprecipitates, indicating an interaction between the two. Therefore, both LOK and SLK are effectors of RhoA.

Collectively, these results suggest a model in which RhoA selectively regulates the apical domain of epithelial cells in a negative feedback loop involving active ERM proteins (Fig. 7 G). RhoA activates both the kinases LOK/SLK and ROCK to mediate phosphorylation of ERM proteins and MLC2, respectively. ROCK also negatively regulates PP1, the phosphatase that dephosphorylates both phospho-MLC (pMLC) and pERMs. pERMs localized exclusively in the apical domain regulate RhoA in a negative feedback loop.

A prediction of this model is that a difference in contractile force should exist between wild-type and knockout cells. Cultured cells treated with calyculin A to elevate the level of myosin-II activity will ultimately contract (Ishihara et al., 1989). Therefore, we examined the contraction of spread LOK$^{-/-}$ SLK$^{-/-}$ and ezrin$^{-/-}$ radixin$^{-/-}$ cells compared with wild-type cells in the presence of 10 nM calyculin A. When wild-type cells were treated with 10 nM calyculin A for 1 h, a few cells showed rounding and detachment from the plate. In a dramatic difference, LOK$^{-/-}$ SLK$^{-/-}$ and ezrin$^{-/-}$ radixin$^{-/-}$ cells showed significant rounding and detachment from neighboring cells in under 30 min (Fig. S5 A and Video 2). This contractility is a result of enhanced myosin-II activity, as the calyculin A–induced contraction was prevented by inclusion of the myosin-II inhibitor blebbistatin, which showed no rounding or contraction in any cell type after 1 h (Fig. S5 B and Video 3). These results are in agreement with Fig. 7, A and B, documenting an increased level of MLC phosphorylation in the knockout cells in the presence of calyculin A. However, calyculin A also results in enhanced phosphorylation of ERMs (Viswanatha et al., 2012), so we wished to examine if the contractility difference induced by calyculin A was present in cells where the level of active ezrin was unchanged. To achieve this, we stably expressed the active phosphomimetic ezrin-T567E in double-knockout cells. The contraction induced by calyculin A was greatly reduced in both LOK$^{-/-}$ SLK$^{-/-}$ and ezrin$^{-/-}$ radixin$^{-/-}$ cells expressing ezrin-T567E (Fig. S5 B and Video 4). This implies that it is the loss of active ERMs, and not the loss of LOK and SLK independent of ERMs, that regulates the contractility due to enhanced RhoA-GTP.

The colon-derived DLD-1 cells also show loss of apical organization and upregulation of active RhoA when ERM or LOK/SLK is knocked out

To explore if the results obtained with the placentally derived epithelial Jeg-3 cells are applicable to other epithelial cells, we made use of the human pseudo-diploid colorectal carcinoma DLD-1 line that has been engineered for inducible expression of Cas9 (McKinley and Cheeseman, 2017). Like Jeg-3 cells, DLD-1 cells express LOK, SLK, ezrin, and radixin, but not moesin (Fig. 8 A). They form a polarized epithelium with apical ezrin, organized tight junctional ZO-1, and actin enrichment at the level of junctions (Fig. 8 B). Transfection of DLD-1 cells to express gRNAs to knock down either ezrin and radixin or LOK and SLK unexpectedly resulted in a mixed population of cells in which many of the cells already exhibited protein loss, presumably due to a low level of Cas9 expression (Fig. 8 A). In these mixed populations, the level of pERMs was greatly diminished (Fig. 8 A). Moreover, microscopic analysis showed dramatic differences between wild-type cells and the mixed knockout populations. In cells lacking ezrin and radixin or LOK and SLK, there is a lack of organized junctional ZO-1 staining, and actin is less organized and not circling the cell at the level of adherens junctions (Fig. 8 B). Examination of the actin staining at higher magnification suggests complete disorganization of the adherens junctions (Fig. 8, B and C), presumably because the induced contractile bundles have torn them apart. As in Jeg-3 cells, active RhoA is enhanced in the knockout cells (Fig. 8, D and E). Thus, as in Jeg-3 cells, loss of active ERMs results in the elevation of RhoA-GTP and disorganization of the apical domain.

Discussion

In this study, we investigated the phenotypes conferred by loss of ERM proteins or their activators, LOK and SLK. In some cells, loss of LOK and SLK, or in fact just ezrin in HeLa or Caco-2 cells, is too unhealthy to maintain, indicating that ERM proteins and their activating kinases can be almost essential. This is consistent in mice, flies, and the nematode worm, where loss of ezrin or the single ERM protein (flies and worm) is lethal (Jankovics et al., 2002; Saotome et al., 2004; van Furden et al., 2004; Göbel et al., 2004). Additionally, the loss of SLK in mouse or the single homologue Slik in the fly is also lethal (Al-Zahrani et al., 2013; Hipfner and Cohen, 2003). Loss of just LOK in the mouse has a more modest phenotype (Belkina et al., 2009), presumably due to the presence of SLK. We were fortunate to start with a cell line, Jeg-3, that can tolerate loss of either all ERM proteins or both LOK and SLK, as this allowed us to study their phenotypes. As far as we are aware, there are the first vertebrate cells isolated genetically lacking either all ERM proteins or the kinases LOK and SLK.

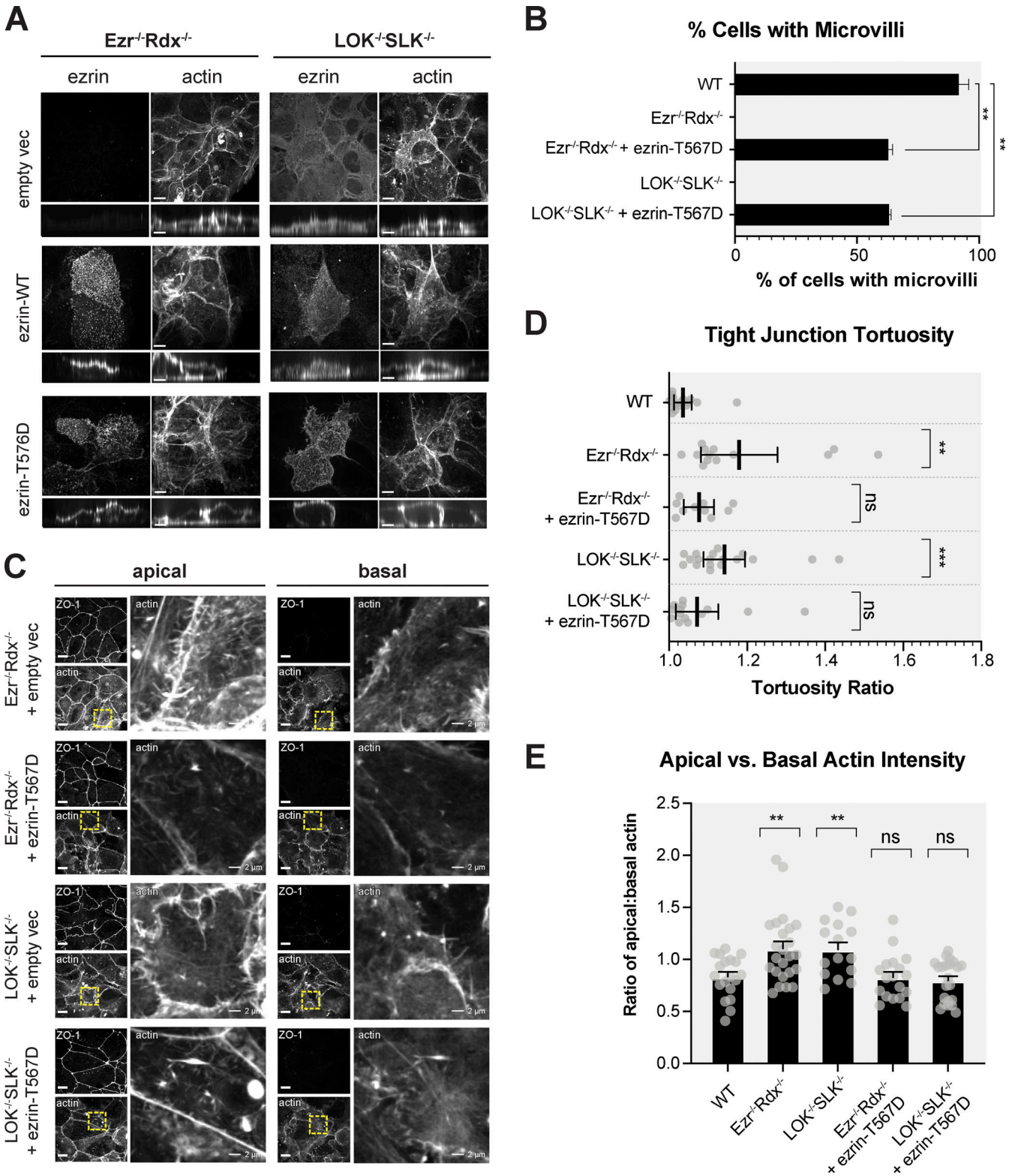

Figure 6. **Constitutively active ezrin rescues apical actin distribution in knockout cells. (A)** Jeg-3–knockout cells expressing empty pCDH vector control, wild-type ezrin, or T567 phosphomimetic were stained for ezrin and actin. Maximum-intensity projections and vertical cross-sections (expanded fourfold for clarity) are shown. **(B)** Percentage of cells expressing microvilli-like structures. Bars represent mean ± SEM; $n = 3$. **(C)** Comparison of ZO-1 and actin between basolateral and apical confocal slices between Jeg-3–knockout cells expressing phosphomimetic ezrin-T567D. Apical Z-slices were determined by the presence of ZO-1. Yellow boxes indicate the region of the image that was expanded on the right. **(D)** Quantification of tight junction tortuosity using ZO-1 staining. $n \geq 10$ cells per condition. Center lines show mean ± SEM. **(E)** The ratios of relative mean actin intensity values per cell between apical and basolateral cross-sections. $n \geq 15$ cells per condition. Bars show mean ± SEM. P values were calculated against wild type with Welch's *t* test (**, $P \leq 0.01$; ***, $P \leq 0.001$). Scale bars, 10 µm unless otherwise noted in magnified images.

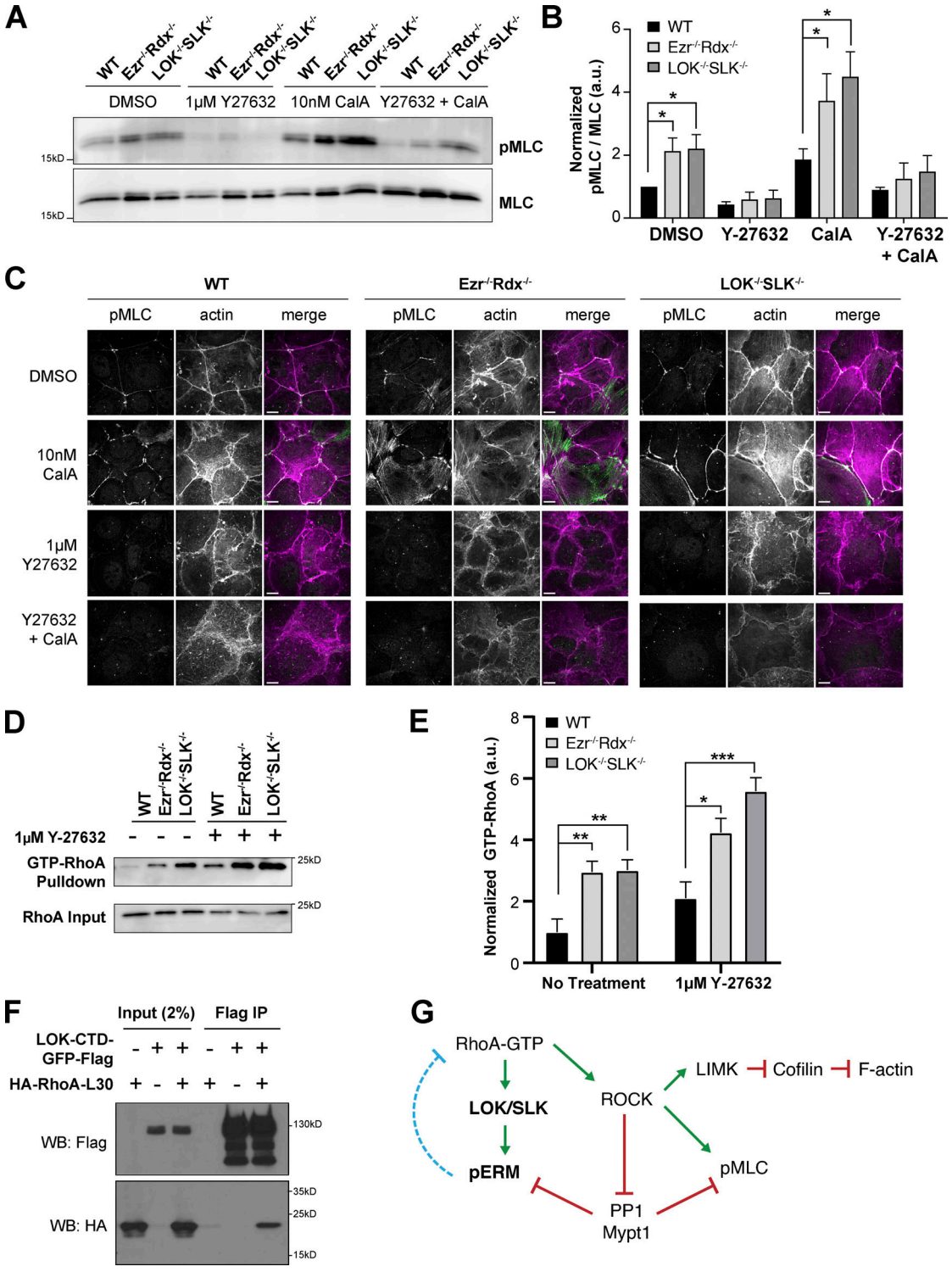

Figure 7. **pERMs negatively regulate myosin activation through RhoA. (A)** Jeg-3 wild-type and knockout cells were either treated with DMSO, 10 nM calyculin A for 10 min, or 1 µM Y-27632 for 30 min or cotreated with 10 nM calyculin A and 1 µM Y-27632 before cell lysate extraction. Extracts were then blotted with pMLC (T18/S19) and total MLC antibodies. **(B)** Quantification of pMLC staining normalized to MLC as a loading control. Bars show mean ± SEM; n = 7 for DMSO and n = 4 for other drug conditions. P values were calculated against wild type using the t test (*, P ≤ 0.05). **(C)** Jeg-3 wild-type and knockout cells treated with either DMSO, 10 nM calyculin A (CalA) for 10 min, or 1 µM Y-27632 for 30 min or cotreated with 10 nM CalA and 1 µM Y-27632 before fixation and staining with pMLC and actin. Images are max Z-projections of apical cross-sections. **(D)** Representative Western blot of active RhoA-GTP pull-down results in Jeg-3 cells. Upper row: RhoA blot of the active fraction of RhoA (GTP) pulled down by rhotekin beads. Lower row: Blot of RhoA of 5% of input lysate. **(E)** Quantification of pull-down represented in D. Mean ± SEM; n = 10 for no treatment and n = 5 for Y-27632 (t test; *, P ≤ 0.05; **, P ≤ 0.01; ***, P ≤ 0.001). **(F)** LOK-CTD-GFP-Flag pull-down of cells expressing constitutively active RhoA (RhoA-L30), indicating that C-terminal LOK binds active RhoA. WB, Western blot. **(G)** Model of RhoA signaling negatively regulated by pERMs (dotted blue line).

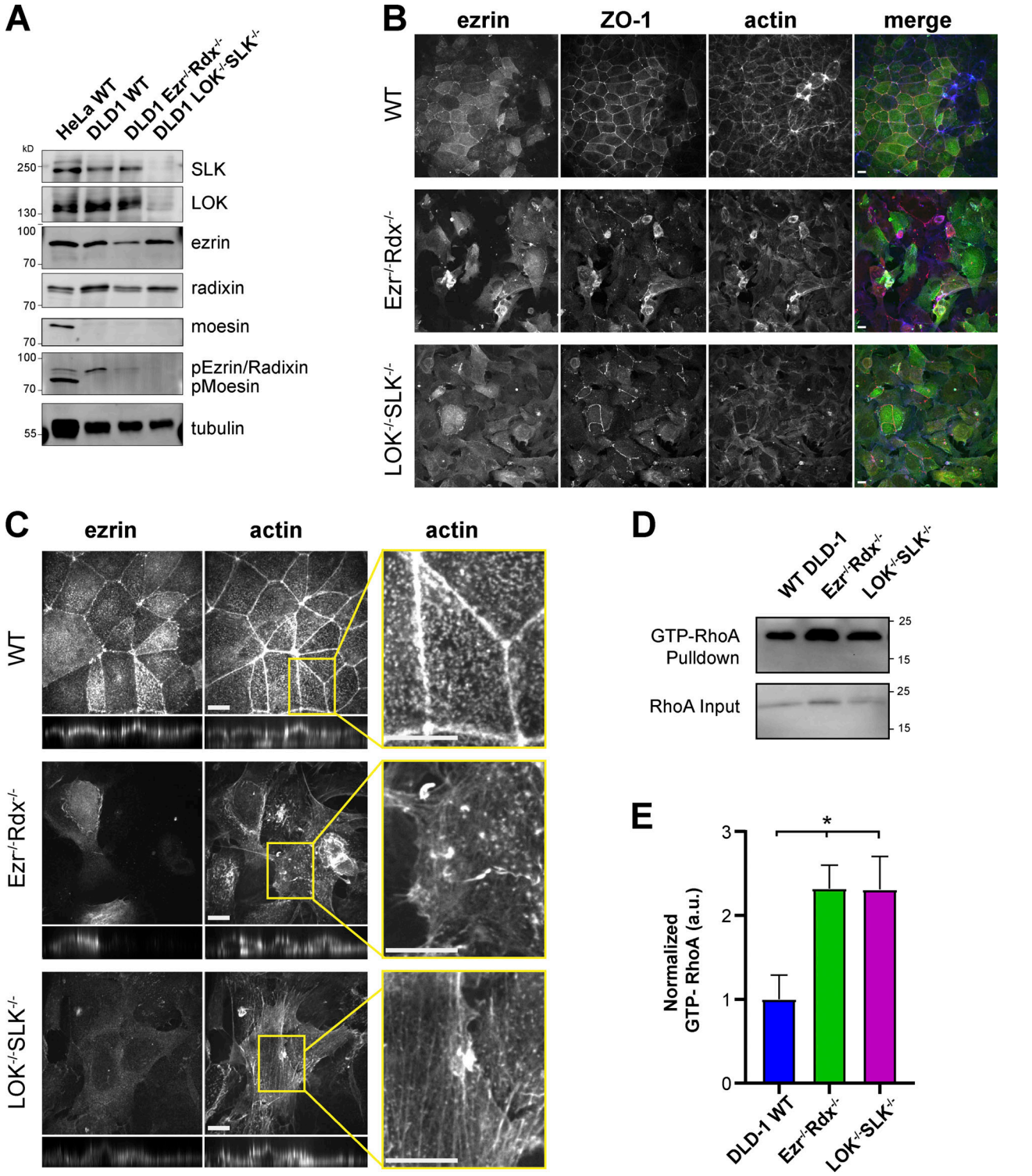

Figure 8. **Loss of ezrin/radixin or LOK/SLK in DLD-1 colon epithelial cells. (A)** Protein expression using the indicated antibodies in Western blots of DLD-1 mixed knockout cell lysates. In DLD-1 LOK$^{-/-}$ SLK$^{-/-}$ cells, pERM is undetected. HeLa cell lysate was used as a control for expression of moesin, which is not present in DLD-1 cells. Tubulin expression was used as a loading control. **(B)** DLD-1 wild-type and mixed knockout populations of Ezr$^{-/-}$ Rdx$^{-/-}$ cells and LOK$^{-/-}$ SLK$^{-/-}$ cells stained with ezrin, ZO-1, and actin at 40× magnification. **(C)** DLD-1 wild-type and mixed knockout populations of Ezr$^{-/-}$ Rdx$^{-/-}$ cells and LOK$^{-/-}$ SLK$^{-/-}$ cells stained with ezrin and actin at 100× magnification. Vertical projections were expanded fourfold for clarity. Magnified insets highlight major differences between actin organization in wild-type and knockout cells. **(D)** Representative Western blot of active RhoA-GTP pull-down results in DLD-1 cells. Upper row: RhoA blot of the active fraction of RhoA-GTP pulled down by rhotekin beads. Lower row: Blot of RhoA of 5% of input lysate. **(E)** Quantification of pull-down represented in D. Mean ± SEM; n = 6 (t test; *, P ≤ 0.05). Scale bars, 10 µm.

Previous studies have shown that wild-type epithelial cells maintain ∼50% of their ezrin in the active, phosphorylated state with cycling between active and inactive states occurring on the scale of ∼2 min (Viswanatha et al., 2012). This balanced system is critical for maintaining a polarized morphology (Viswanatha et al., 2012) and is consistent with mislocalization, overexpression, and hyperphosphorylation of ezrin found in types of human cancers (reviewed in Clucas and Valderrama, 2014). Our finding that loss of LOK and SLK results in ablation of all detectable ezrin-T567 phosphorylation is consistent with LOK and SLK being the major, if not only, kinases that can phosphorylate the ERM regulatory threonine (T567 in ezrin). This result is in agreement with earlier descriptions that Slik is solely responsible for the activation of fly moesin (Hipfner et al., 2004).

A remarkable aspect of our results is that cells lacking either all ERM proteins or LOK and SLK are phenotypically very similar. Both grow slower, have lost all apical microvilli, have greatly reduced junctional actin but also an aberrantly high level of apical F-actin and myosin, have wavy cell junctions, have a stiffer apical domain, contract abnormally in the presence of the phosphatase calyculin A, and have elevated levels of Rho-GTP. This raises the question whether the ERM proteins are the sole substrate of LOK/SLK. An intricate multistep mechanism is involved in phosphorylation of ezrin by LOK. It requires priming of ezrin by phosphatidylinositol 4,5-bisphosphate, then insertion of the C-terminal region of LOK between the ezrin FERM and C-terminal F-actin binding domain, which gives access for the kinase domain to bind a recognition site and ultimately phosphorylate T567 (Pelaseyed et al., 2017). This mechanism, together with the strong preference for tyrosine two residues upstream of the targeted threonine (Belkina et al., 2009), makes phosphorylation of ERM proteins highly selective. This selectivity coupled with the ability of mutationally active ezrin (ezrin-T567D) to suppress the phenotype of LOK/SLK cells strongly supports the notion that ERM proteins are the major functional substrates. Using a phosphoproteomics approach in unpublished work, we sought to identify additional LOK/SLK substrates. While we encountered many phosphopeptides whose level was elevated in wild-type cells compared with LOK/SLK-knockout cells, none had the appropriate LOK/SLK consensus sequence. Therefore, LOK/SLK and ERM proteins appear to work together as a functional unit. Although we were not able to identify additional LOK/SLK substrates, technical limitations may have obscured them from our analysis. In support of this possibility, the phenotypes of LOK/SLK cells enumerated above were almost always more severe than in the ERM-knockout cells. Thus, the possibility remains that there is another minor substrate of LOK/SLK performing a function redundant with ERM proteins.

While we expected to see loss of microvilli in cells lacking ERM proteins, we were surprised to encounter an extensive actin/myosin-II network in the apical domain replacing the junctional and microvillar actin. This phenotype was also seen in LOK/SLK-knockout cells, implying that active ERM proteins can regulate the myosin and actin distribution in the apical domain. RhoA-GTP is known to positively regulate nonmuscle myosin-II activity through ROCK as well as F-actin turnover through LIM kinase and cofilin. Since both actin turnover and myosin contractility are altered in the absence of pERMs, we then considered a possible overactivation of RhoA in the knockout cells. Indeed, the level of RhoA-GTP was significantly elevated in both ERM- and LOK/SLK-knockout cells. Thus, active ERMs are negative regulators of RhoA (Fig. 7 G).

There have been several indications of a connection between ERM protein function and RhoA. First, ROCK1 was reported as the kinase that phosphorylates ERM proteins, in part because ROCK1 overexpression resulted in formation of microvilli in cos-7 cells and its reported ability to phosphorylate radixin in vitro (Matsui et al., 1998; Oshiro et al., 1998). With the findings that Mypt1/PP1 is the phosphatase responsible for dephosphorylating ERM proteins (Fukata et al., 1998) and that Mypt1/PP1 is negatively regulated by ROCK1 (Velasco et al., 2002), the earlier result can be explained. In the fly, phenotypes resulting from loss of moesin can be rescued by reducing the level of RhoA (Speck et al., 2003). Recent work has shown that RhoA-GTP directly dimerizes and activates SLK (Bagci et al., 2020). In the work of Bagci et al., the appearance of increased apical contractile fibers was not observed following the single knockdown of either LOK or SLK, in concurrence with our finding that only double knockout of both kinases resulted in the most severe observed phenotypes. As pERM proteins act as negative regulators of RhoA-GTP, a local feedback cycle exists in which RhoA-GTP and pERMs regulate each other's activity specifically across the apical domain (Fig. 7 G).

RhoA is a well-recognized spatial regulator of the adherens junctions between epithelial cells (reviewed in Hartsock and Nelson, 2008; Marjoram et al., 2014; McCormack et al., 2013). Active RhoA is highly enriched at junctions through the action of various regulators, including the RhoA-GEFs (RhoA guanine nucleotide exchange factors) p114RhoGEF and ECT2, and indirectly through active myo-IIA recruitment of ROCK1 to phosphorylate and inactivate the ability of Rnd3 to recruit p190B RhoA-GAP (RhoA GTPase-activating protein; Ratheesh et al., 2012; Reyes et al., 2014; Terry et al., 2011; Priya et al., 2015; Lecuit and Yap, 2015). Misregulation of RhoA can affect the mechanical tension between junctions of neighboring epithelial cells (Zihni et al., 2014). Indeed, this is what we observed by knocking out active ERMs. As a consequence of removing active ERMs, F-actin bundles are redistributed away from the junctions and into actomyosin networks across the apical terminal web. This state can be mimicked in wild-type epithelial cells by introducing an actin-stabilizing drug such as jasplakinolide. Conversely, the actin in knockout cells can be redirected back toward junctions by adding actin-depolymerizing drug latrunculin B. A similar phenomenon is seen when anillin is manipulated in epithelial cells, where anillin-knockdown cells produce low tensile forces and overexpression produces high tensile forces due to misregulation of medial-apical F-actin (Arnold et al., 2019). Thus, local spatial regulation of proteins like ERMs and anillin can influence the RhoA-dependent actin turnover at the apical domain and junctions of epithelial cells. As LOK is an effector of active RhoA and is located in the microvilli, and not the cell–cell junctions, a subpopulation of RhoA must be specifically regulated across the apical surface of epithelial cells. The activity of this local RhoA subpopulation is negatively

regulated by pERM proteins, presumably through either a Rho-GEF or a Rho-GAP. In the fly Rho-GAP, Conundrum has been shown to bind moesin and act as a negative regulator of Rho1. However, since deletion of Conundrum has no obvious phenotype, there is likely functional redundancy with another Rho-GAP (Neisch et al., 2013). Our future work will be aimed at identifying the factor(s) that allow active ERMs to mediate local negative regulation of RhoA-GTP.

The negative signaling pathway from active ERMs to RhoA that we have uncovered in the placentally derived Jeg-3 cells appears to also operate in the epithelial colon-derived DLD-1 cells, as loss of ERMs or LOK/SLK from these cells also results in elevated RhoA-GTP levels and a highly disrupted apical domain. Therefore, the negative regulation of RhoA in the apical domain by active ERMs is likely a common feature of epithelial cells.

In summary, ERM proteins and their activators LOK/SLK function in the same pathway as a unit to build microvilli on the apical surface of epithelial cells and locally modulate the level of RhoA-GTP in a feedback inhibition cycle. The next challenge will be to understand how this feedback loop is regulated and restricted to the apical domain.

Materials and methods

Reagents and cDNAs

Ezrin antibodies were either a mouse anti-ezrin antibody (CPTC-ezrin-1 supernatant concentrate obtained from the Developmental Studies Hybridoma Bank; catalog no. CPTC-Ezrin-1; Research Resource Identification AB_2100318) used at 1:1,250 (Western blot) or 1:100 (immunofluorescence) or a previously characterized rabbit polyclonal antibody raised against full-length human ezrin (Bretscher, 1989) and used at 1:1,000 (Western blot) or 1:200 (immunofluorescence). Rabbit anti-EBP50 was also a previously characterized antibody (Reczek et al., 1997) and was used at 1:50 (immunofluorescence). Mouse anti–ZO-1 (BD Biosciences; catalog no. 610966) was used at 1:100 (immunofluorescence). Rabbit anti-radixin (Cell Signaling Technology; catalog no. C4G7) was used at 1:1,000 (Western blot) to blot for both radixin (80 kD) and moesin (75 kD). Rabbit anti-pERM (raised against recombinant phosphopeptide) was used at 1:1,000 (Western blot). Rabbit anti-LOK (catalog no. A300-400A) used at 1:500 (Western blot) and rabbit anti-SLK (catalog no. A300-500A) used at 1:100 (Western blot) were purchased from Bethyl Laboratories, Inc. For immunofluorescence of LOK, a homemade rabbit polyclonal antibody raised against LOK-586-stop (Pocono Rabbit Farm) was used at 1:50. Mouse anti-Flag (Sigma-Aldrich; catalog no. F1804) was used at 1:5,000 (Western blot), and mouse anti-tubulin (Sigma-Aldrich; catalog no. T5168) was used at 1:5,000 (Western blot). Mouse anti-GFP used at 1:100 (immunofluorescence) was obtained from Santa Cruz Biotechnology, Inc. (catalog no. SC-9996). Rabbit antibodies for anti-MLC2 (catalog no. 3672) and anti–phospho-MLC2 (raised against phospho-Thr18/Ser19; catalog no. 3674) were purchased from Cell Signaling Technology and used at 1:500 (Western blot) and 1:50 (immunofluorescence). Mouse anti–E-cadherin mAb was purchased from BD Transduction Laboratories (catalog no. 610181) and used at 1:100 for immunofluorescence. Mouse anti-RhoA antibody (Cytoskeleton Inc.; catalog no. ARH05) was obtained through Cytoskeleton Inc., and the RhoA Activation Assay Biochem Kit was used at 1:500. Rabbit antibody for anti–nonmuscle myo-IIB from BioLegend (catalog no. 909902) and nonmuscle myo-IIA (BioLegend; catalog no. 909802) were used at 1:100 (Western blot and immunofluorescence). Rabbit polyclonal antibodies raised by standard procedures against vinculin, brush border myosin-II, and α-actinin purified from chicken gizzard were used at 1:2,000, 1:200, or 1:200, respectively, for Western blotting (Fig. S2). The myosin antibody was described in Bretscher (1989). The vinculin and α-actinin antibodies were described in Franck et al. (1990). For actin staining, Alexa Fluor 488 (Invitrogen; catalog no. A12379) or Alexa Fluor 647 phalloidin (Invitrogen; catalog no. A30107) was used at 1:250. WGA conjugated to Alexa Fluor 488 (Invitrogen; catalog no. W11261) was used at 1:300 to stain cell membranes.

Phos-tag was purchased from Wako Chemicals. Jasplakinolide (catalog no. 11705) and Y-27632 (catalog no. 100005583-5) were purchased from Cayman Chemicals. DMSO (catalog no. D2650), latrunculin B (catalog no. L5288), and cytochalasin D (catalog no. C8273) were purchased from Sigma-Aldrich. Calyculin A (catalog no. BML-El92-0100) was purchased from Enzo Life Sciences, and blebbistatin (catalog no. B592500) was purchased from Toronto Research Chemicals.

Ezrin point mutants T567E and T567A were previously generated as described in Viswanatha et al. (2012). Sequences for LOK-GFP-Flag, LOK-CTD-GFP-Flag, and LOK-K65R-GFP-Flag were previously generated in the laboratory (Pelaseyed et al., 2017; Viswanatha et al., 2012). To generate stable cell lines, ezrin and LOK cDNAs were subcloned into pCDH lentivector (System Biosciences). The puromycin gene in pCDH was then substituted for blasticidin using Gibson assembly. The lentivectors were then transfected with psPAX2 and pCMV-VSV-G before virus collection and transduction into Jeg-3 cells. Cells were then grown under blasticidin selection at 5.0 µg/ml for 1–2 wk before immunofluorescence experiments. Stable expression for ezrin was validated using either an ezrin antibody for ezrin constructs or GFP expression for LOK constructs.

Cell culture

Jeg-3, HeLa, and Caco-2 cells (American Type Culture Collection) were maintained in a 5% CO_2 humidified chamber at 37°C. Jeg-3 cells were maintained in MEM with 10% FBS, penicillin/streptomycin, and GlutaMAX (Thermo Fisher Scientific). Cells were cultured on Corning 100 × 20-mm cell culture polystyrene dishes. HeLa and Caco-2 cells were maintained in DMEM with 10% FBS and penicillin/streptomycin. Knockout cell lines were maintained with additional 2.0 µg/ml puromycin (Sigma-Aldrich) selection. Transient transfections were done using either Lipofectamine 3000 (Invitrogen) according to the manufacturer's instructions or polyethylenimine reagent (PolyPlus) as previously described (Viswanatha et al., 2012).

Single-guide RNAs (sgRNAs) were designed using CRISPR analysis tools on Benchling and cloned into puromycin-resistant pLenti-CRISPRV2 (Addgene; catalog no. 49535) or pLenti-sgRNA

(a gift from the Cheeseman laboratory; Whitehead Institute, Cambridge, MA) as described in Sanjana et al. (2014) and Shalem et al. (2014). The following sgRNA sequences were used: 5′-GCA ATGTCCGAGTTACCACCA-3′ (ezrin), 5′-AGAAGCAGAACGACT TGAAA-3′ (radixin), 5′-CAGTGTGCGTGTGACCACCA-3′ (moesin), 5′-GTAAGACTCACCCAGCATGA-3′ (LOK), and 5′-GCAGTA CGAACACGTGAAGA-3′ (SLK). Each lentiviral construct was then transfected into 293TN cells with psPAX3 and pCMV-VSV-G (a gift from Jan Lammerding, Weill Institute for Cell and Molecular Biology, Cornell University, Ithaca, NY) for 48–72 h before virus collection. Target cells (Jeg-3, HeLa, or Caco-2) were then transduced with either one or two lentiviruses in order to generate a mixed population of single- and double-knockout cells. Cells were sorted into single cells and then expanded in puromycin selection before screening by immunofluorescence and Western blotting.

Growth curves of Jeg-3 cells were performed by plating cells on low-evaporation-lid, flat-bottom, 96-well plates (Corning; catalog no. 3595). Once plated, cells were seeded at 3,000 cells per well. Plates were then imaged once per hour for 100 h using a 20× objective using an Incucyte ZOOM v2016 (Essen BioScience) kept in standard cell incubation chamber conditions. Raw data images were collected and analyzed using Incucyte. Graphs were assembled and exported using GraphPad Prism (version 8).

Statistical methods

The statistical tests applied, the number of independent data points (n), and the definition of error bars are described in the figure legends specific to the tested data. Additional analysis is described in the Materials and methods sections pertaining to specific techniques. All t tests were performed as two-tailed tests. For parametric tests, data distributions were assumed to be normal, but this was not formally tested.

Western blotting and immunoprecipitation

Western blot analysis of cell lysates was done using 6–12% split SDS-PAGE gels, while 6% gel was used for Phos-tag experiments. Phos-tag reagent was added at a final concentration of 50 µM to a standard Tris-glycine-SDS polyacrylamide gel according to the manufacturer's recommendations. Gels were transferred to a polyvinylidene difluoride (PVDF) membrane and blocked with 5% milk in TBS + 0.5% Tween-20. Primary antibodies were incubated with the membrane in 5% BSA either for 1 h at room temperature or overnight at 4°C. Bands were detected with HRP (Thermo Fisher Scientific; catalog no. 31460) or infrared fluorescent secondary antibodies (Invitrogen or LI-COR Biosciences; catalog nos. 926-32221 and 926-32210). Membranes were imaged using a scanner (Odyssey; LI-COR Biosciences). Blots imaged using HRP were imaged using a Bio-Rad ChemiDoc. Band intensities were calculated using ImageJ's gels toolkit. GraphPad Prism was used for statistical analysis of gel band intensity quantification.

For detecting MLC and pMLC, 16% or split 7.5–17.5% SDS-PAGE gels were used and transferred to PVDF membranes with 0.2-µm pore size (EMD Millipore; Immobilon-P^{SQ}). The membrane was then blocked with Immobilon Block-PO phosphoprotein-blocking buffer (EMD Millipore; catalog no. WBAVDP001) and incubated with primary antibody solution overnight before developing with chemiluminescent reagents (Radiance Q Plus, catalog no. AC2101; Azure Biosystems) on a Bio-Rad ChemiDoc imaging system. Relative band intensities were calculated in ImageJ and normalized to a loading control and exported to GraphPad Prism for statistical analysis. Calyculin A treatments for MLC blotting were performed by incubating the drug with cells for 10 min at 37°C before lysis. Lysis of cells for MLC blotting was performed with warm (70°C) Laemmli sample buffer, followed by immediate scraping and boiling.

To determine an interaction between LOK and constitutively active RhoA-L30, cells were transiently cotransfected with LOK-CTD-GFP-Flag and HA-RhoA-L30 (a kind gift from the Cerione laboratory, Cornell University, Ithaca, NY). After 24 h, cells were lysed and then solubilized in cold immunoprecipitation buffer (25 mM Tris, pH 7.4, 5% glycerol, 150 mM NaCl, 50 mM NaF, 0.1 mM Na_3VO_4, 10 mM β-glycerol phosphate, 8.7 mg/ml para-nitrophenylphosphate, 0.5% Triton X-100, 0.1 µM calyculin A, and protease inhibitor tablet [Roche]) and immunoprecipitated for 2 h using Flag M2 affinity gel (Sigma-Aldrich; catalog no. F2426). Immunoprecipitates were then extensively washed in immunoprecipitation wash buffer (25 mM Tris, pH 7.4, 5% glycerol, 150 mM NaCl, 50 mM NaF, and 0.2% Triton X-100) and then eluted in 200 µg/ml 3× Flag peptide, denatured in Laemmli buffer, resolved by SDS-PAGE, transferred to PVDF, and developed with HRP Western blot detection.

Active RhoA pull-down assay

For GTP-RhoA pull-down assay, the Rho Activation Assay Biochem Kit (Cytoskeleton Inc.; catalog no. BK036) was used as described in the product manual. In summary, wild-type Jeg-3 or knockout cell lines were plated and grown for 3 d on Corning 100 × 20-mm cell culture polystyrene dishes. An optimal confluency of 70–80% was used, as higher confluences can result in partial loss of a monolayer and disruption of apical morphology in Jeg-3 cells. For Y-27632 drug treatments, drug was diluted to a 100× stock in water and then stored in experimental sized aliquots at −20°C. Prior to drug treatment, Y27632 was diluted into media and added to the cells to a final concentration of 1 µg/ml for 1 h at 37°C. After 1 h, both drug-treated and untreated cells were placed on ice and washed three times with ice-cold PBS. Cells were lysed using the kit lysis buffer and protease inhibitor cocktail, then clarified at 10,000 × g at 4°C for 1 min. The lysate was then snap frozen in liquid nitrogen as quickly as possible to reduce RhoA-GTP hydrolysis. Frozen lysates were then stored at −80°C. Protein concentrations were measured using the Bradford reagent and absorption at 595 nm. Upon thawing aliquots, lysate protein concentration was then normalized to a uniform protein concentration using kit lysis buffer. Equal concentrations of lysate were then passed on 100 µg rhotekin Rho-binding domain beads and incubated at 4°C for 1 h under agitation. The beads were then washed, pelleted, and finally boiled with 20 µl Laemmli sample buffer. Positive and negative controls using wild-type Jeg-3 lysate were incubated with either GTPγs or GDP for 15 min before passing over the rhotekin Rho-binding domain beads. These controls were used to confirm the detectable range of Western blot

detection, RhoA hydrolysis activity, and rhotekin bead binding capacity. Samples were run on a 7.5–17.5% split SDS-PAGE gel and blotted for RhoA; Monoclonal Mouse anti-RhoA antibody (Cytoskeleton Inc.; catalog no. ARH05) was used at 1:500 dilution in TBS with Tween overnight, and anti-mouse HRP secondary antibody was used at 1:10,000. Western blots were analyzed using the ImageJ gel analysis toolkit. Pull-down intensity values were normalized to their respective input or loading band intensity, averaged across replicates, then reported as a ratio relative to the wild-type to no-treatment condition. SEM was calculated by propagation of error using the Δ method for this transformation to an average normalized ratio. For statistical significance analysis, an unpaired *t* test was used.

Time-lapse microscopy, immunofluorescence, and image analysis

Cells were treated to a final concentration of 10 nM calyculin A diluted into cell media plus 10 mM Hepes at the start of time-lapse imaging. Phase-contrast images for time-course videos were taken every 4 min for 1 h using a 20× objective on a Zeiss AXIO widefield inverted microscope fitted with a 37°C temperature environmental chamber. For blebbistatin experiments, blebbistatin was added to the media to a final concentration of 25 µM 30 min before addition of calyculin A. For calyculin A treatment time-course videos and still frames, imaging was started immediately before addition of calyculin A, and time 0 was defined as the first captured frame after calyculin A addition.

Prior to fixation for immunofluorescence, Jeg-3 cells grown on coverslips were washed with PBS and prestained with WGA at 1:300 for 30 min. For actin turnover experiments in Fig. 5 A, Jeg-3 cells were treated with either DMSO, 500 nM jasplakinolide, or 100 ng/ml latrunculin B for 30 min before fixation. For detecting endogenous localization of LOK, cells were fixed for 10 min in 3.7% formalin in a cytoskeletal stabilizing buffer (S Buffer: 0.1 M PIPES, 5 mM EGTA, 4% poly ethylene glycol, pH 6.9) supplemented with 250 nM calyculin A. After fixation, cells were permeabilized in 0.2% Triton X-100 in S Buffer, blocked with immunofluorescence buffer (cytoskeletal stabilizing buffer + 0.5% BSA + 0.5% goat serum + 0.1% Triton X-100) for 10 min. Otherwise, for all other immunofluorescent experiments, cells grown on glass coverslips were fixed in 3.7% formalin/PBS for 15 min at room temperature. Cells were then washed with PBS and blocked with immunofluorescence buffer (PBS + 0.5% BSA + 0.5% goat serum + 0.1% Triton X-100) for 10 min. Primary and secondary antibodies were then applied in immunofluorescence buffer containing 2% FBS. Alexa Fluor–conjugated phalloidin was added to the secondary. The cells were mounted in SlowFade Diamond Antifade (Thermo Fisher Scientific) and imaged using a spinning-disk (Yokogawa CSU-X1; Intelligent Imaging Innovations) Leica DMi600B microscope with a spherical aberration correction device and a 100×/1.46 NA or 40×/1.30 NA Leica objective. All fixed-cell imaging was done at room temperature (23°C). Images were acquired with a metal-oxide semiconductor device Hamamatsu ORCA-Flash 4.0 camera (scientific complementary metal–oxide–semiconductor), and image slices were assembled using SlideBook 6 software (Intelligent Imaging Innovations). Maximum- or summed-intensity projections were assembled in SlideBook 6 and exported to Illustrator software (Adobe). For clarity, side projections were vertically expanded using Illustrator. Line scan analysis was performed within ImageJ using the Plot Profile toolkit. Intensity values were then imported into either GraphPad Prism or RStudio for graphing. An 8-pixel sliding window average and normalization of intensity to the minimum-intensity value was applied to line scans of actin SIM imaging to reduce noise and allow comparison between conditions.

Live-cell imaging of ZO-1–GFP (Addgene; catalog no. 30313) was performed by transiently transfecting Jeg-3 cells 24 h before imaging. Immediately before imaging, cell medium was changed to FluoroBrite DMEM (Thermo Fischer Scientific; catalog no. A1896701) with 10% FBS, and cells were kept in a 5% CO_2 humidified environmental chamber at 37°C throughout imaging. Cells were imaged every 10 min for >15 h using an inverted Leica DMi8 widefield microscope equipped with a Leica 40×/0.95 NA air objective, a Leica DFC 9000 GTC camera, Leica Application Suite X THUNDER deconvolution software, and Leica adaptive focus control. Deconvolution images of myo-IIA were performed on the above Leica DMi8 widefield microscope, Leica Application Suite X THUNDER deconvolution software, and Leica adaptive focus control. Default small sample Leica THUNDER deconvolution settings were used, except for adjustment of structure size to 1,000 nm and reduction of the deconvolution strength to 30%.

SIM was performed on a Zeiss Elyra super-resolution inverted Axio Observer.Z1 microscope through the Cornell Institute of Biotechnology Imaging Facility. Illumination was performed using 405-, 488-, 561-, and 640-nm lasers though a 63×/1.4 NA oil objective and captured on a pco.edge 5.5m camera. Exposure time was sample and channel dependent to optimize SIM reconstruction but ranged from 50 to 400 ms. Z-slice steps were set to the optimized minimum for each illumination channel calculated through the ZEN black software. Grating for SIM was set to five rotations in all conditions, and processing was done though the automatic SIM processing toolset within the ZEN software using default settings. Color channels were corrected for chromatic aberration by applying the built-in color alignment ZEN software to a Z-stack of images of the 100-nm multicolor beads from an Invitrogen Molecular Probes TetraSpeck Fluorescent Microspheres Size Kit (catalog no. T14792).

The presence or absence of microvilli was scored as described previously (Garbett et al., 2010; Hanono et al., 2006; LaLonde et al., 2010; Pelaseyed et al., 2017; Sauvanet et al., 2015). More than 50 cells per replicate were stained using the WGA, ezrin, and phalloidin and binned into two categories: microvilli and no microvilli. Microvilli above cell–cell junctions were ignored in the scoring.

For calculating tortuosity among tight junctions and relative apical and lateral actin intensities, cells were stained with a ZO-1 antibody and phalloidin and imaged on a spinning-disk microscope as described earlier. To analyze tortuosity, the ZO-1 channel was skeletonized into 1-pixel line widths using ImageJ. Between two consecutive intersection points, a straight-line length was measured, and the average of two manually traced line lengths (to

account for human variability) along the skeletonized line was also measured. From there, the ratio of the actual line length to the expected line length (straight length) was calculated and exported into GraphPad Prism for statistical analysis. For comparing actin intensities between apical and lateral regions, Max-Z projections were divided between ZO-1–positive (apical) and ZO-1–negative (lateral) staining. From there, outlines of each cell were traced and measured for their relative mean intensity value in the apical stacks versus the lateral stacks. The ratios between the apical and lateral values were then calculated, plotted, and analyzed for statistical significance (Welch's *t* test) in GraphPad Prism.

AFM

AFM experiments were performed using an MFP-3D-BIO atomic force microscope (Asylum Research) mounted on an Olympus IX71 inverted microscope residing on a Herzan AVI 350-S Active Vibration Isolation Table totally enclosed in an airtight BCH-45 Large Acoustic Isolation Hood. Software modules were written in Igor Pro by Wavemetrics. Cells were plated onto a WillCo-dish glass-bottom dish (size 50 × 7 mm, glass 30 mm, class 1.5, 0.17 mm, product no. GWST-5030; Willco Wells). Pyramidal-shaped probe tips (PNP-TR-20) from Asylum Research (804.NW.PNP-TR) were used and calibrated using an in-air calculation of the spring constant. Individual cells within monolayers were selected using phase-contrast live imaging with the probe tip location simultaneously illuminated onto the field of view. Probe tips were lowered onto a cell at a velocity of 1,000 nm/s to a trigger point of 1 nN. Individual cells were force mapped by indenting 100 times over a square 20 × 20-µm area. Simultaneous force indentation and membrane retraction measurements were made by first incubating probe tips with 3.0 mg/ml concanavalin A in PBS buffer for 1.5 h at room temperature. Deflection and z-probe position data were exported into MATLAB and then analyzed using the open access software from Huth et al. (2019), modified for a pyramidal-shaped probe tip. Force indentation traces were filtered for single force peaks, then chi-value goodness fit to the Hertz model. Young's modulus statistical analysis and graphing of AFM data were performed in GraphPad Prism.

Online supplemental material

Fig. S1 shows single-knockout phenotypes in Jeg-3 cells. Fig. S2 shows tight junction formation and adherence junction phenotypes, including still frames from Video 1, and basal or focal contact protein images and expression in Jeg-3 wild-type and knockout cells. Fig. S3 shows myo-IIA localization and the effect of myosin-II inhibition by blebbistatin on tight junctions. Fig. S4 shows the effects of actin, cytochalasin D, latrunculin B, and jasplakinolide on Jeg-3 wild-type and knockout cells. Fig. S5 shows still frames from Videos 2, 3, and 4 supporting the indication that pERMs negatively regulate myosin contractility. Video 1 shows a time-course movie of live Jeg-3 wild-type, $Ezr^{-/-}$ $Rdx^{-/-}$, and $LOK^{-/-}$ $SLK^{-/-}$ cells transfected with ZO-1–GFP tight junction marker. Video 2 shows a time-course movie of Jeg-3 wild-type, $Ezr^{-/-}$ $Rdx^{-/-}$, and $LOK^{-/-}$ $SLK^{-/-}$ cells treated with 10 nM calyculin A over 1 h. Video 3 shows a time-course movie of Jeg-3 wild-type, $Ezr^{-/-}$ $Rdx^{-/-}$, and $LOK^{-/-}$ $SLK^{-/-}$ cells treated with 10 nM calyculin A and 25 µM blebbistatin over 1 h. Video 4 shows a time-course movie of $Ezr^{-/-}$ $Rdx^{-/-}$ and $LOK^{-/-}$ $SLK^{-/-}$ cells transfected with phosphomimetic ezrin (ezrin-T567E) treated with 10 nM calyculin A over 1 h.

Acknowledgments

We thank the University of Vermont Larner College of Medicine Microscopy Imaging Center and the Cornell Institute of Biotechnology Imaging Facility for use of AFM and SIM equipment, respectively. We thank S. Nelson, A. Howe, S. Huth, and A. Martin for their helpful discussions and J. Lammerding for use of reagents. We thank I. Cheeseman for providing DLD-1 cells. We appreciate the effort by S. Marshall and M. Smolka in their attempts to identify additional LOK phosphorylation targets.

This work was supported by National Institutes of Health grants R01 GM036552 and R35 GM131751 to A. Bretscher and the Sam and Nancy Fleming Research Fellowship to A. Lombardo. The University of Vermont Larner College of Medicine Microscopy Imaging Center is supported by a National Institutes of Health award (S10RR025498), and the Cornell Institute of Biotechnology Imaging Facility is supported by National Science Foundation funding (1428922).

The authors declare no competing financial interests.

Author contributions: A. Bretscher, C. Sauvanet, R. Zaman, and A. Lombardo conceptualized the study. A. Bretscher, R. Zaman, and A. Lombardo wrote the manuscript. C. Sauvanet, R. Zaman, V. Awad, L.E.-R. Bonomo, and D. McDermitt generated knockout cell lines. R. Zaman performed microvilli, actin, and tight junction image analysis. A. Lombardo performed SIM imaging, AFM analysis, and RhoA-GTP pulldowns. R. Viswanatha performed LOK pulldown assays.

Submitted: 27 July 2020
Revised: 7 February 2021
Accepted: 9 March 2021

References

Al-Zahrani, K., K. Baron, and L. Sabourin. 2013. Ste20-like kinase SLK, at the crossroads: A matter of life and death. *Cell Adh. Migr.* 7(1):1–10. https://doi.org/10.4161/cam.22495

Amano, M., M. Ito, K. Kimura, Y. Fukata, K. Chihara, T. Nakano, Y. Matsuura, and K. Kaibuchi. 1996. Phosphorylation and activation of myosin by Rho-associated kinase (Rho-kinase). *J. Biol. Chem.* 271:20246–20249. https://doi.org/10.1074/jbc.271.34.20246

Arber, S., F.A. Barbayannis, H. Hanser, C. Schneider, C.A. Stanyon, O. Bernard, and P. Caroni. 1998. Regulation of actin dynamics through phosphorylation of cofilin by LIM-kinase. *Nature.* 393:805–809. https://doi.org/10.1038/31729

Arnold, T.R., J.H. Shawky, R.E. Stephenson, K.M. Dinshaw, T. Higashi, F. Huq, L.A. Davidson, and A.L. Miller. 2019. Anillin regulates epithelial cell mechanics by structuring the medial-apical actomyosin network. *eLife.* 8:e39065. https://doi.org/10.7554/eLife.39065

Bagci, H., N. Sriskandarajah, A. Robert, J. Boulais, I.E. Elkholi, V. Tran, Z.-Y.Y. Lin, M.-P.P. Thibault, N. Dubé, D. Faubert, et al. 2020. Mapping the proximity interaction network of the Rho-family GTPases reveals signalling pathways and regulatory mechanisms. *Nat. Cell Biol.* 22:120–134. https://doi.org/10.1038/s41556-019-0438-7

Baumgartner, M., A.L. Sillman, E.M. Blackwood, J. Srivastava, N. Madson, J.W. Schilling, J.H. Wright, and D.L. Barber. 2006. The Nck-interacting kinase phosphorylates ERM proteins for formation of lamellipodium by growth factors. *Proc. Natl. Acad. Sci. USA.* 103:13391–13396. https://doi.org/10.1073/pnas.0605950103

Belkina, N.V., Y. Liu, J.-J.J. Hao, H. Karasuyama, and S. Shaw. 2009. LOK is a major ERM kinase in resting lymphocytes and regulates cytoskeletal rearrangement through ERM phosphorylation. *Proc. Natl. Acad. Sci. USA.* 106:4707–4712. https://doi.org/10.1073/pnas.0805963106

Bonilha, V.L., S.C. Finnemann, and E. Rodriguez-Boulan. 1999. Ezrin promotes morphogenesis of apical microvilli and basal infoldings in retinal pigment epithelium. *J. Cell Biol.* 147:1533–1548. https://doi.org/10.1083/jcb.147.7.1533

Bretscher, A. 1989. Rapid phosphorylation and reorganization of ezrin and spectrin accompany morphological changes induced in A-431 cells by epidermal growth factor. *J. Cell Biol.* 108:921–930. https://doi.org/10.1083/jcb.108.3.921

Clucas, J., and F. Valderrama. 2014. ERM proteins in cancer progression. *J. Cell Sci.* 127:267–275. https://doi.org/10.1242/jcs.133108

Fehon, R.G., A.I. McClatchey, and A. Bretscher. 2010. Organizing the cell cortex: the role of ERM proteins. *Nat. Rev. Mol. Cell Biol.* 11:276–287. https://doi.org/10.1038/nrm2866

Franck, Z., M. Footer, and A. Bretscher. 1990. Microinjection of villin into cultured cells induces rapid and long-lasting changes in cell morphology but does not inhibit cytokinesis, cell motility, or membrane ruffling. *J. Cell Biol.* 111:2475–2485. https://doi.org/10.1083/jcb.111.6.2475

Fukata, Y., K. Kimura, N. Oshiro, H. Saya, Y. Matsuura, and K. Kaibuchi. 1998. Association of the myosin-binding subunit of myosin phosphatase and moesin: dual regulation of moesin phosphorylation by Rho-associated kinase and myosin phosphatase. *J. Cell Biol.* 141:409–418. https://doi.org/10.1083/jcb.141.2.409

Garbett, D., D.P. LaLonde, and A. Bretscher. 2010. The scaffolding protein EBP50 regulates microvillar assembly in a phosphorylation-dependent manner. *J. Cell Biol.* 191:397–413. https://doi.org/10.1083/jcb.201004115

Gary, R., and A. Bretscher. 1995. Ezrin self-association involves binding of an N-terminal domain to a normally masked C-terminal domain that includes the F-actin binding site. *Mol. Biol. Cell.* 6:1061–1075. https://doi.org/10.1091/mbc.6.8.1061

Gloerich, M., J.P. ten Klooster, M.J. Vliem, T. Koorman, F.J. Zwartkruis, H. Clevers, and J.L. Bos. 2012. Rap2A links intestinal cell polarity to brush border formation. *Nat. Cell Biol.* 14:793–801. https://doi.org/10.1038/ncb2537

Göbel, V., P.L. Barrett, D.H. Hall, and J.T. Fleming. 2004. Lumen morphogenesis in *C. elegans* requires the membrane-cytoskeleton linker *erm-1*. *Dev. Cell.* 6:865–873. https://doi.org/10.1016/j.devcel.2004.05.018

Haas, M.A., J.C. Vickers, and T.C. Dickson. 2007. Rho kinase activates ezrin-radixin-moesin (ERM) proteins and mediates their function in cortical neuron growth, morphology and motility in vitro. *J. Neurosci. Res.* 85:34–46. https://doi.org/10.1002/jnr.21102

Hall, A. 1998. Rho GTPases and the actin cytoskeleton. *Science.* 279:509–514. https://doi.org/10.1126/science.279.5350.509

Hall, A., and C.D. Nobes. 2000. Rho GTPases: molecular switches that control the organization and dynamics of the actin cytoskeleton. *Philos. Trans. R. Soc. Lond. B Biol. Sci.* 355:965–970. https://doi.org/10.1098/rstb.2000.0632

Hanono, A., D. Garbett, D. Reczek, D.N. Chambers, and A. Bretscher. 2006. EPI64 regulates microvillar subdomains and structure. *J. Cell Biol.* 175:803–813. https://doi.org/10.1083/jcb.200604046

Hartsock, A., and W.J. Nelson. 2008. Adherens and tight junctions: structure, function and connections to the actin cytoskeleton. *Biochim. Biophys. Acta.* 1778:660–669. https://doi.org/10.1016/j.bbamem.2007.07.012

Hayashi, K., S. Yonemura, T. Matsui, and S. Tsukita. 1999. Immunofluorescence detection of ezrin/radixin/moesin (ERM) proteins with their carboxyl-terminal threonine phosphorylated in cultured cells and tissues. *J. Cell Sci.* 112:1149–1158.

Hipfner, D.R., and S.M. Cohen. 2003. The *Drosophila* sterile-20 kinase slik controls cell proliferation and apoptosis during imaginal disc development. *PLoS Biol.* 1:e35. https://doi.org/10.1371/journal.pbio.0000035

Hipfner, D.R., N. Keller, and S.M. Cohen. 2004. Slik Sterile-20 kinase regulates Moesin activity to promote epithelial integrity during tissue growth. *Genes Dev.* 18:2243–2248. https://doi.org/10.1101/gad.303304

Huth, S., S. Sindt, and C. Selhuber-Unkel. 2019. Automated analysis of soft hydrogel microindentation: Impact of various indentation parameters on the measurement of Young's modulus. *PLoS One.* 14:e0220281. https://doi.org/10.1371/journal.pone.0220281

Ishihara, H., B.L. Martin, D.L. Brautigan, H. Karaki, H. Ozaki, Y. Kato, N. Fusetani, S. Watabe, K. Hashimoto, D. Uemura, et al. 1989. Calyculin A and okadaic acid: inhibitors of protein phosphatase activity. *Biochem. Biophys. Res. Commun.* 159:871–877. https://doi.org/10.1016/0006-291X(89)92189-X

Jankovics, F., R. Sinka, T. Lukácsovich, and M. Erdélyi. 2002. MOESIN crosslinks actin and cell membrane in *Drosophila* oocytes and is required for OSKAR anchoring. *Curr. Biol.* 12:2060–2065. https://doi.org/10.1016/S0960-9822(02)01256-3

Jin, H., T. Sperka, P. Herrlich, and H. Morrison. 2006. Tumorigenic transformation by CPI-17 through inhibition of a merlin phosphatase. *Nature.* 442:576–579. https://doi.org/10.1038/nature04856

Kimura, K., M. Ito, M. Amano, K. Chihara, Y. Fukata, M. Nakafuku, B. Yamamori, J. Feng, T. Nakano, K. Okawa, et al. 1996. Regulation of myosin phosphatase by Rho and Rho-associated kinase (Rho-kinase). *Science.* 273:245–248. https://doi.org/10.1126/science.273.5272.245

Kuramochi, S., T. Moriguchi, K. Kuida, J. Endo, K. Semba, E. Nishida, and H. Karasuyama. 1997. LOK is a novel mouse STE20-like protein kinase that is expressed predominantly in lymphocytes. *J. Biol. Chem.* 272:22679–22684. https://doi.org/10.1074/jbc.272.36.22679

LaLonde, D.P., D. Garbett, and A. Bretscher. 2010. A regulated complex of the scaffolding proteins PDZK1 and EBP50 with ezrin contribute to microvillar organization. *Mol. Biol. Cell.* 21:1519–1529. https://doi.org/10.1091/mbc.e10-01-0008

Lecuit, T., and A.S. Yap. 2015. E-cadherin junctions as active mechanical integrators in tissue dynamics. *Nat. Cell Biol.* 17:533–539. https://doi.org/10.1038/ncb3136

Loomis, P.A., L. Zheng, G. Sekerková, B. Changyaleket, E. Mugnaini, and J.R. Bartles. 2003. Espin cross-links cause the elongation of microvillus-type parallel actin bundles in vivo. *J. Cell Biol.* 163:1045–1055. https://doi.org/10.1083/jcb.200309093

Maekawa, M., T. Ishizaki, S. Boku, N. Watanabe, A. Fujita, A. Iwamatsu, T. Obinata, K. Ohashi, K. Mizuno, and S. Narumiya. 1999. Signaling from Rho to the actin cytoskeleton through protein kinases ROCK and LIM-kinase. *Science.* 285:895–898. https://doi.org/10.1126/science.285.5429.895

Marjoram, R.J., E.C. Lessey, and K. Burridge. 2014. Regulation of RhoA activity by adhesion molecules and mechanotransduction. *Curr. Mol. Med.* 14:199–208. https://doi.org/10.2174/1566524014666140128104541

Matsui, T., M. Maeda, Y. Doi, S. Yonemura, M. Amano, K. Kaibuchi, S. Tsukita, and S. Tsukita. 1998. Rho-kinase phosphorylates COOH-terminal threonines of ezrin/radixin/moesin (ERM) proteins and regulates their head-to-tail association. *J. Cell Biol.* 140:647–657. https://doi.org/10.1083/jcb.140.3.647

Matsui, T., S. Yonemura, S. Tsukita, and S. Tsukita. 1999. Activation of ERM proteins in vivo by Rho involves phosphatidyl-inositol 4-phosphate 5-kinase and not ROCK kinases. *Curr. Biol.* 9:1259–1262. https://doi.org/10.1016/S0960-9822(99)80508-9

McCormack, J., N.J. Welsh, and V.M.M. Braga. 2013. Cycling around cell-cell adhesion with Rho GTPase regulators. *J. Cell Sci.* 126:379–391. https://doi.org/10.1242/jcs.097923

McKinley, K.L., and I.M. Cheeseman. 2017. Large-scale analysis of CRISPR/Cas9 cell-cycle knockouts reveals the diversity of p53-dependent responses to cell-cycle defects. *Dev. Cell.* 40:405–420.e2. https://doi.org/10.1016/j.devcel.2017.01.012

Meenderink, L.M., I.M. Gaeta, M.M. Postema, C.S. Cencer, C.R. Chinowsky, E.S. Krystofiak, B.A. Millis, and M.J. Tyska. 2019. Actin dynamics drive microvillar motility and clustering during brush border assembly. *Dev. Cell.* 50:545–556.e4. https://doi.org/10.1016/j.devcel.2019.07.008

Nakamura, H., S. Kimura, S. Kenmotsu, H. Sakai, T. Saku, and H. Ozawa. 1995. Immunolocalization of CD44 and Heparan Sulfate Chains on the Stratum Intermedium and Papillary Layer in the Rat Enamel Organ. *Arch. Histol. Cytol.* 58(3):323–334. https://doi.org/10.1679/aohc.58.323

Neisch, A., E. Formstecher, and R. Fehon. 2013. Conundrum, an ARHGAP18 orthologue, regulates RhoA and proliferation through interactions with Moesin. *Mol. Biol. Cell.* 24(9):1420–1433. https://doi.org/10.1091/mbc.E12-11-0800

Ng, T., M. Parsons, W. Hughes, J. Monypenny, D. Zicha, A. Gautreau, M. Arpin, S. Gschmeissner, P. Verveer, P. Bastiaens, et al. 2001. Ezrin is a downstream effector of trafficking PKC-integrin complexes involved in the control of cell motility. *EMBO.* 20(11):2723–2741. https://doi.org/10.1093/emboj/20.11.2723

Oshiro, N., Y. Fukata, and K. Kaibuchi. 1998. Phosphorylation of moesin by Rho-associated kinase (Rho-kinase) plays a crucial role in the formation of microvilli-like structures. *J. Biol. Chem.* 273:34663–34666. https://doi.org/10.1074/jbc.273.52.34663

Pakkanen, R., K. Hedman, O. Turunen, T. Wahlström, and A. Vaheri. 1987. Microvillus-specific Mr 75,000 plasma membrane protein of human choriocarcinoma cells. *J. Histochem. Cytochem.* 35:809–816. https://doi.org/10.1177/35.8.3298422

Pearson, M.A., D. Reczek, A. Bretscher, and P.A. Karplus. 2000. Structure of the ERM protein moesin reveals the FERM domain fold masked by an extended actin binding tail domain. *Cell.* 101:259–270. https://doi.org/10.1016/S0092-8674(00)80836-3

Pelaseyed, T., R. Viswanatha, C. Sauvanet, J.J. Filter, M.L. Goldberg, and A. Bretscher. 2017. Ezrin activation by LOK phosphorylation involves a PIP_2-dependent wedge mechanism. *eLife.* 6:e22759. https://doi.org/10.7554/eLife.22759

Pietromonaco, S.F., P.C. Simons, A. Altman, and L. Elias. 1998. Protein kinase C-θ phosphorylation of moesin in the actin-binding sequence. *J. Biol. Chem.* 273:7594–7603. https://doi.org/10.1074/jbc.273.13.7594

Priya, R., G.A. Gomez, S. Budnar, S. Verma, H.L. Cox, N.A. Hamilton, and A.S. Yap. 2015. Feedback regulation through myosin II confers robustness on RhoA signalling at E-cadherin junctions. *Nat. Cell Biol.* 17:1282–1293. https://doi.org/10.1038/ncb3239

Ratheesh, A., G.A. Gomez, R. Priya, S. Verma, E.M. Kovacs, K. Jiang, N.H. Brown, A. Akhmanova, S.J. Stehbens, and A.S. Yap. 2012. Centralspindlin and α-catenin regulate Rho signalling at the epithelial zonula adherens. *Nat. Cell Biol.* 14:818–828. https://doi.org/10.1038/ncb2532

Reczek, D., M. Berryman, and A. Bretscher. 1997. Identification of EBP50: A PDZ-containing phosphoprotein that associates with members of the ezrin-radixin-moesin family. *J. Cell Biol.* 139:169–179. https://doi.org/10.1083/jcb.139.1.169

Reyes, C.C., M. Jin, E.B. Breznau, R. Espino, R. Delgado-Gonzalo, A.B. Goryachev, and A.L. Miller. 2014. Anillin regulates cell-cell junction integrity by organizing junctional accumulation of Rho-GTP and actomyosin. *Curr. Biol.* 24:1263–1270. https://doi.org/10.1016/j.cub.2014.04.021

Rodriguez-Boulan, E., and I.G. Macara. 2014. Organization and execution of the epithelial polarity programme. *Nat. Rev. Mol. Cell Biol.* 15:225–242. https://doi.org/10.1038/nrm3775

Sanjana, N.E., O. Shalem, and F. Zhang. 2014. Improved vectors and genome-wide libraries for CRISPR screening. *Nat. Methods.* 11:783–784. https://doi.org/10.1038/nmeth.3047

Saotome, I., M. Curto, and A.I. McClatchey. 2004. Ezrin is essential for epithelial organization and villus morphogenesis in the developing intestine. *Dev. Cell.* 6:855–864. https://doi.org/10.1016/j.devcel.2004.05.007

Sauvanet, C., D. Garbett, and A. Bretscher. 2015. The function and dynamics of the apical scaffolding protein E3KARP are regulated by cell-cycle phosphorylation. *Mol. Biol. Cell.* 26:3615–3627. https://doi.org/10.1091/mbc.E15-07-0498

Shalem, O., N.E. Sanjana, E. Hartenian, X. Shi, D.A. Scott, T. Mikkelson, D. Heckl, B.L. Ebert, D.E. Root, J.G. Doench, et al. 2014. Genome-scale CRISPR-Cas9 knockout screening in human cells. *Science.* 343:84–87. https://doi.org/10.1126/science.1247005

Speck, O., S.C. Hughes, N.K. Noren, R.M. Kulikauskas, and R.G. Fehon. 2003. Moesin functions antagonistically to the Rho pathway to maintain epithelial integrity. *Nature.* 421:83–87. https://doi.org/10.1038/nature01295

ten Klooster, J.P., M. Jansen, J. Yuan, V. Oorschot, H. Begthel, V. Di Giacomo, F. Colland, J. de Koning, M.M. Maurice, P. Hornbeck, et al. 2009. Mst4 and Ezrin induce brush borders downstream of the Lkb1/Strad/Mo25 polarization complex. *Dev. Cell.* 16:551–562. https://doi.org/10.1016/j.devcel.2009.01.016

Terry, S.J., C. Zihni, A. Elbediwy, E. Vitiello, I.V. Leefa Chong San, M.S. Balda, and K. Matter. 2011. Spatially restricted activation of RhoA signalling at epithelial junctions by p114RhoGEF drives junction formation and morphogenesis. *Nat. Cell Biol.* 13:159–166. https://doi.org/10.1038/ncb2156

Tran Quang, C., A. Gautreau, M. Arpin, and R. Treisman. 2000. Ezrin function is required for ROCK-mediated fibroblast transformation by the Net and Dbl oncogenes. *EMBO J.* 19:4565–4576. https://doi.org/10.1093/emboj/19.17.4565

van Furden, D., K. Johnson, C. Segbert, and O. Bossinger. 2004. The *C. elegans* ezrin-radixin-moesin protein ERM-1 is necessary for apical junction remodelling and tubulogenesis in the intestine. *Dev. Biol.* 272:262–276. https://doi.org/10.1016/j.ydbio.2004.05.012

Velasco, G., C. Armstrong, N. Morrice, S. Frame, and P. Cohen. 2002. Phosphorylation of the regulatory subunit of smooth muscle protein phosphatase 1M at Thr850 induces its dissociation from myosin. *FEBS Lett.* 527:101–104. https://doi.org/10.1016/S0014-5793(02)03175-7

Viswanatha, R., P.Y. Ohouo, M.B. Smolka, and A. Bretscher. 2012. Local phosphocycling mediated by LOK/SLK restricts ezrin function to the apical aspect of epithelial cells. *J. Cell Biol.* 199:969–984. https://doi.org/10.1083/jcb.201207047

Yang, N., O. Higuchi, K. Ohashi, K. Nagata, A. Wada, K. Kangawa, E. Nishida, and K. Mizuno. 1998. Cofilin phosphorylation by LIM-kinase 1 and its role in Rac-mediated actin reorganization. *Nature.* 393:809–812. https://doi.org/10.1038/31735

Zihni, C., M.S. Balda, and K. Matter. 2014. Signalling at tight junctions during epithelial differentiation and microbial pathogenesis. *J. Cell Sci.* 127:3401–3413. https://doi.org/10.1242/jcs.145029

JCB

Supplemental material

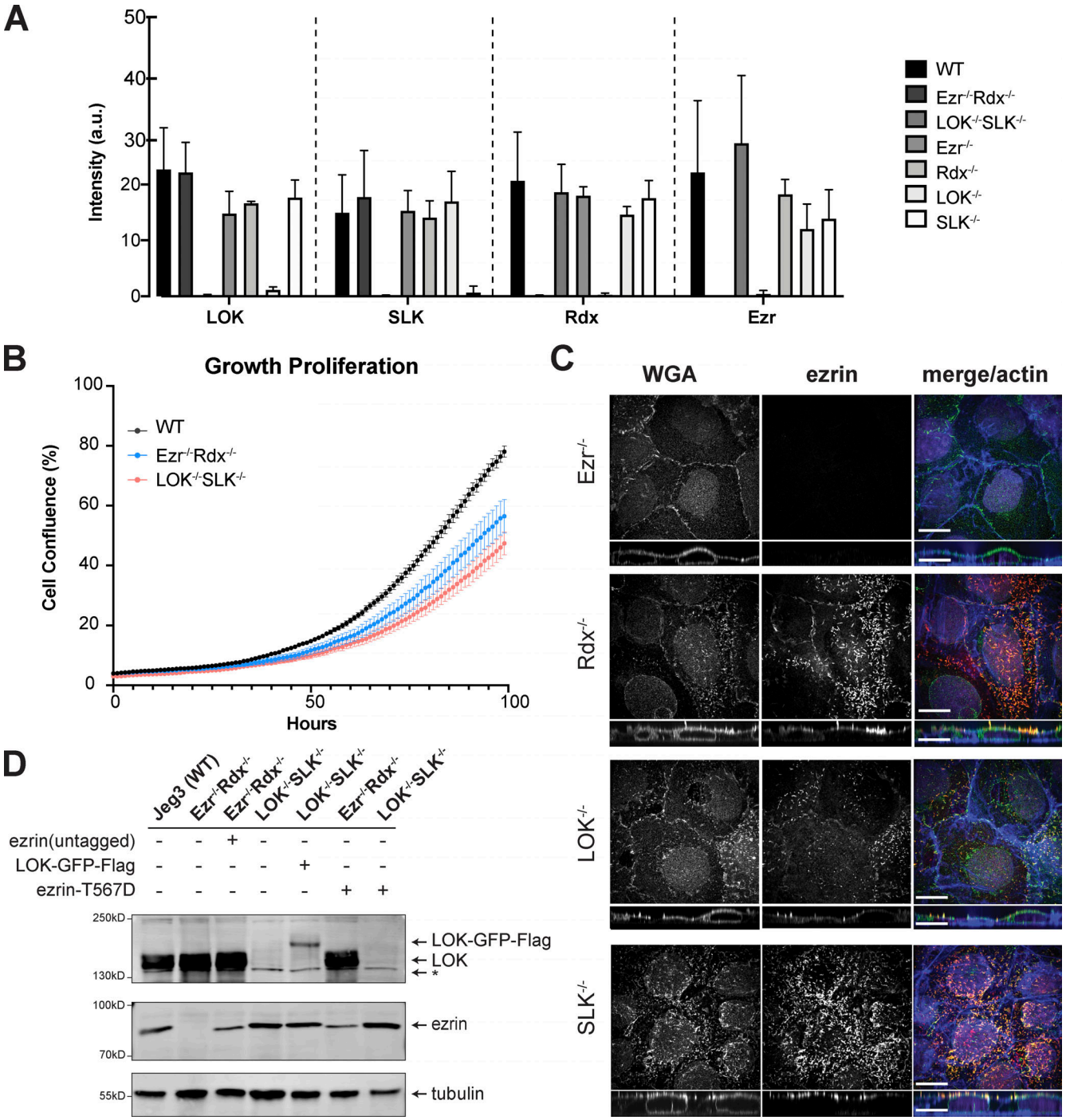

Figure S1. **Single-knockout phenotypes in Jeg-3 cells. (A)** Analysis of protein expression of ERM proteins and LOK/SLK kinases in Jeg-3 single and double CRISPR cell lines. Analysis was based on Western blots using specific primary antibodies for LOK, SLK, radixin, and ezrin. Band intensity measurements were calculated in ImageJ and normalized to tubulin loading control. No significant differences between protein expression were found, suggesting that there is no upregulation of individual ERMs or LOK/SLK kinases in the absence of each. $n = 3$. **(B)** Growth curve wild-type (gray) versus Ezr$^{-/-}$ Rdx$^{-/-}$ (blue) and LOK$^{-/-}$ SLK$^{-/-}$ cells (orange). $n = 15$ wells of cells shown, wild type; $n = 15$, Ezr$^{-/-}$ Rdx$^{-/-}$; $n = 15$, LOK$^{-/-}$ SLK$^{-/-}$. 3,000 cells were seeded per well on 96-well plates and imaged every hour using the Incucyte live-cell analysis system. Each point represents cell confluence, measured by Incucyte over time per hour from 0 to 100 h. Error bars, SEM. **(C)** Representative immunofluorescence staining of microvilli in single-knockout cells used for microvilli quantification and assessment of partial defects. Scale bars, 10 µm. **(D)** Western blots showing expression of ezrin and LOK constructs in Jeg-3 cells. Asterisk indicates the presence of a nonspecific band.

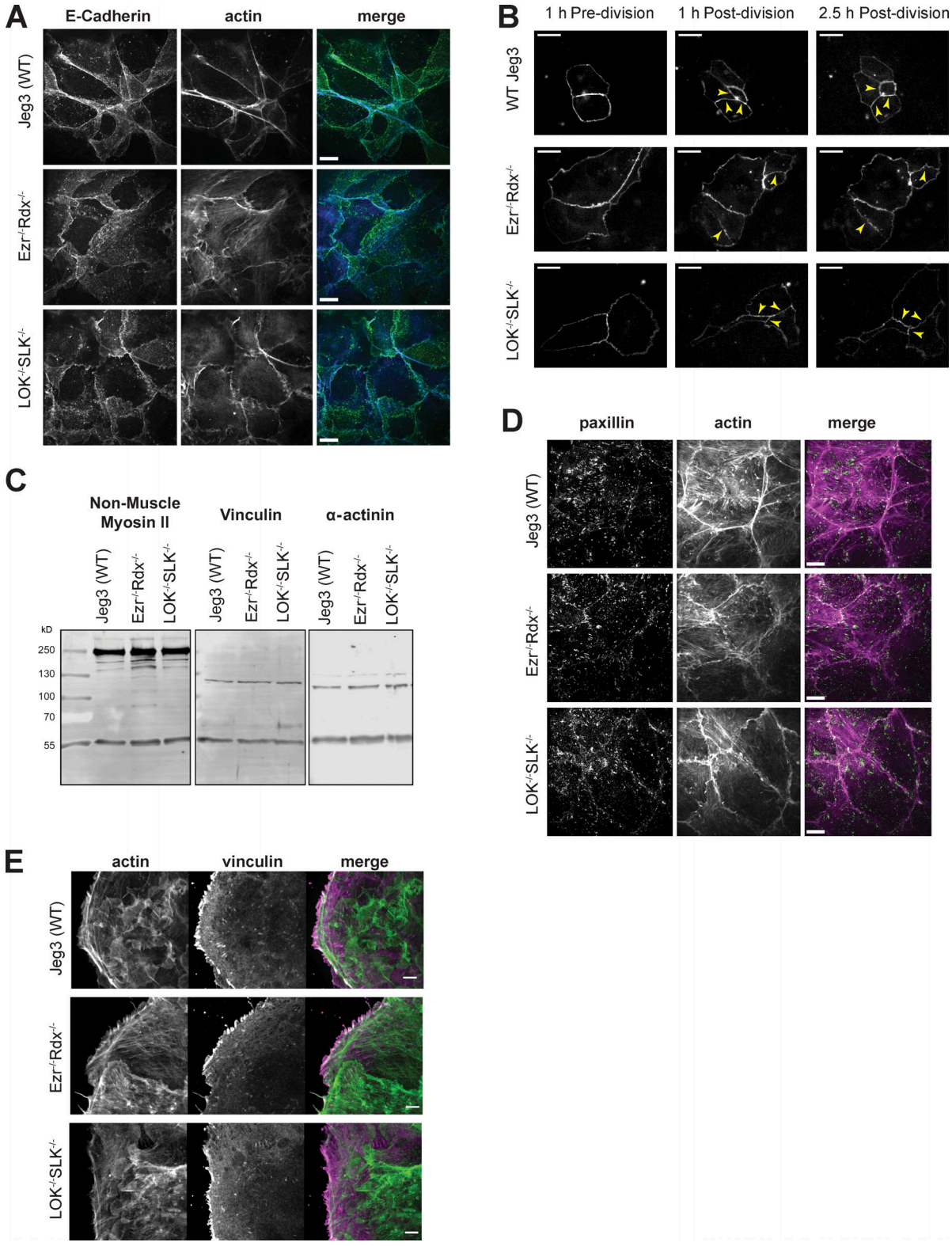

Figure S2. **Tight junction structure and formation and basal contact comparison between Jeg-3 wild-type and knockout cells. (A)** Apical Z-projections of Jeg-3 wild-type and knockout cells stained with E-cadherin and actin. **(B)** Still frames from Video 1 of Jeg-3 cells transfected with ZO-1–GFP showing the development of tight junctions. Following cell division, new junctions are formed that look similar between wild-type and knockout cells (yellow arrowheads; 1 h after division). Over time (2.5 h after division), these same junctions (yellow arrowheads) increase in tortuosity in the knockout cells but are maintained as relatively straight (low tortuosity) in the wild-type cells. **(C)** Western blotting of nonmuscle myosin-II, vinculin, α-actinin, and tubulin in Jeg-3 wild-type and double-knockout cells show similar levels of expression. **(D)** Immunofluorescence staining of paxillin focal adhesion marker and actin shows similar organization. **(E)** Immunofluorescence staining of actin and vinculin indicates that localization of vinculin is similar between knockout cells and Jeg-3 wild-type cells. Scale bars, 10 µm in A, 20 µm in B, 10 µm in D, 5 µm in E.

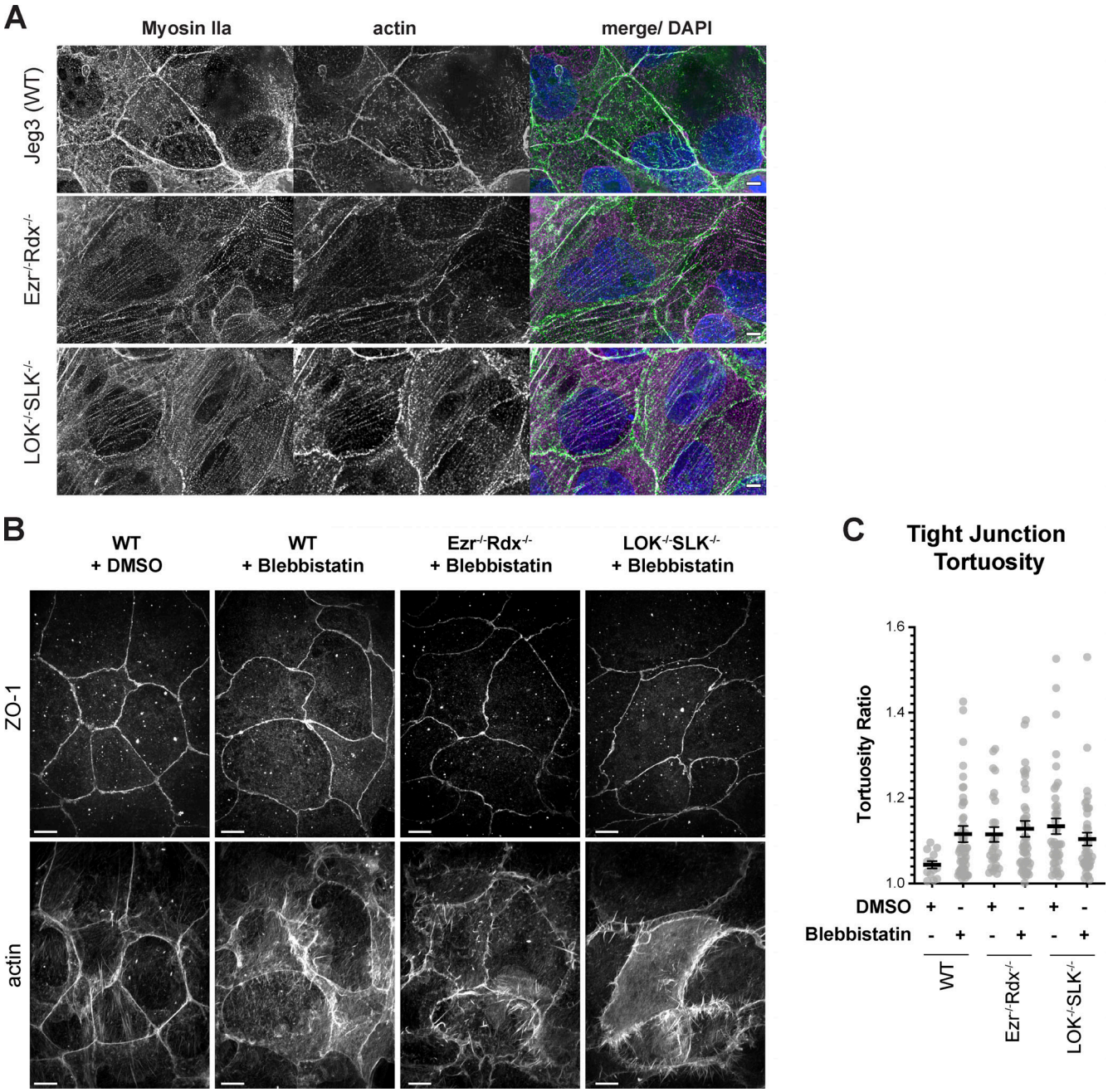

Figure S3. **Imaging of junctional and apical defects with myo-IIA localization and inhibition by blebbistatin. (A)** Deconvolution immunofluorescence staining of myo-IIA shows a similar organization to myo-IIB (Fig. 4). Nonmuscle myo-IIA and myo-IIB are localized to aberrant apical contractile fibers. **(B)** Jeg-3 wild-type and knockout cells were treated with 25 µM blebbistatin for 30 min before immunofluorescence staining of ZO-1 and actin. Images are maximum-intensity projections of apical Z-slices as determined by ZO-1 signal. **(C)** Quantification of tight junction tortuosity using ZO-1 staining. Each point represents the tortuosity from one tight junction intersection to the next intersection. Center lines represent mean ± SEM; $n \geq 13$. Scale bars, 5 µm in A, 10 µm in B.

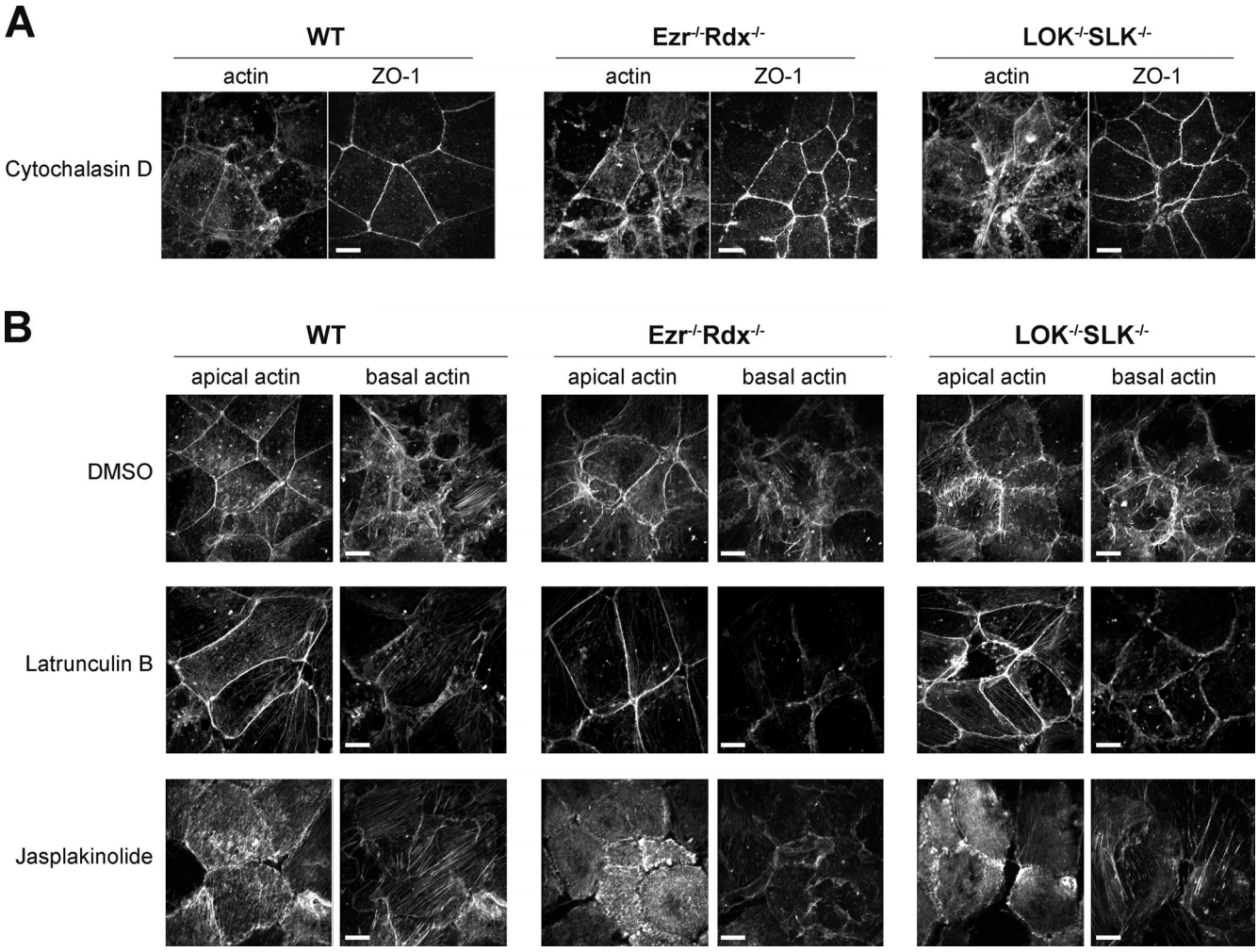

Figure S4. **Effects of actin-polymerizing drugs on Jeg-3 epithelial cells. (A)** Jeg-3 cells treated with 1 µg/ml cytochalasin D for 30 min before fixation and staining with ZO-1 and actin. **(B)** Actin staining of apical and basolateral slices from maximum-intensity projection images in Fig. 5 A. Notably, latrunculin B treatment favors disassembly of basolateral actin over apical actin while maintaining a strong presence of junctional actin. Scale bars, 10 µm.

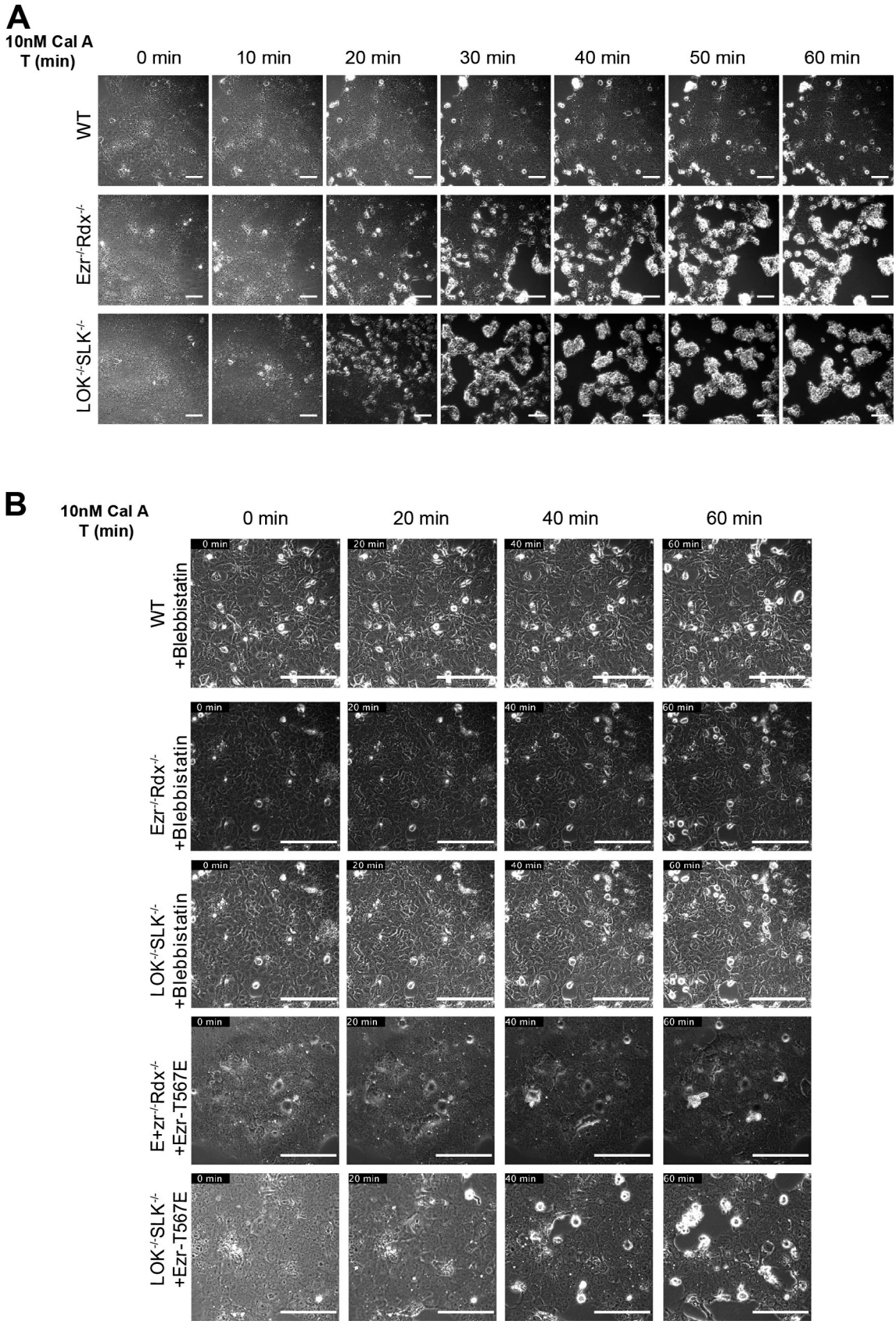

Figure S5. **pERMs negatively regulate myosin contractility. (A)** Representative phase-contrast still images from Video 2 showing the effect of 10 nM calyculin A on wild-type or knockout cells. **(B)** Same as A, except for 30-min treatment with 25 µM blebbistatin (Video 3) or transfection to express phosphomimetic ezrin-T567E (Video 4) before calyculin A treatment. Scale bars, 100 µm.

Video 1. **Development of ZO-1 junctions in Jeg-3 cells.** 15-h time-course movie of Jeg-3 wild-type, Ezr$^{-/-}$ Rdx$^{-/-}$, and LOK$^{-/-}$ SLK$^{-/-}$ cells transfected with ZO-1–GFP. Forces from neighboring cells are applied to the cell–cell contacts. Following division, the development of new tight junctions occurs. Over time, the forces applied to these junctions distort the ZO-1 organization in the knockout cells, but less so in the wild-type cells. Playback speed, 10 frames per second. Scale bars, 20 µm.

Video 2. **Time-course movie of Jeg-3 wild-type, Ezr$^{-/-}$ Rdx$^{-/-}$, and LOK$^{-/-}$ SLK$^{-/-}$ cells treated with 10 nM calyculin A over 1 h.** Playback speed, 10 frames per second. Scale bars, 100 µm.

Video 3. **Time-course movie of Jeg-3 wild-type, Ezr$^{-/-}$ Rdx$^{-/-}$, and LOK$^{-/-}$ SLK$^{-/-}$ cells treated with 10 nM calyculin A and 25 µM blebbistatin over 1 h.** Blebbistatin treatment was added 30 min before video start. Playback speed, 5 frames per second. Scale bars, 100 µm.

Video 4. **Time-course movie of Ezr$^{-/-}$ Rdx$^{-/-}$ and LOK$^{-/-}$ SLK$^{-/-}$ cells transfected with phosphomimetic ezrin (ezrin-T567E) treated with 10 nM calyculin A over 1 h.** Playback speed, 5 frames per second. Scale bars, 100 µm.